Higher buckling and lateral buckling strength of unrestrained and braced thin-walled beams: Analytical, numerical and design approach applications

Hamaidia Achref, Foudil Mohri, Bouzerira Cherif

HIGHER BUCKLING AND LATERAL BUCKLING STRENGTH OF UNRESTRAINED AND BRACED THIN-WALLED BEAMS. ANALYTICAL, NUMERICAL AND DESIGN APPROACH APPLICATIONS.

Achref Hamaidia [1,2], Foudil Mohri [1,*] Cherif Bouzerira [2]

(1): Laboratoire d'Etude des Microstructures et de Mécanique des Matériaux (LEM3), CNRS UMR 7239.Université de Lorraine. 7 rue Félix Savart, BP 15082, 57073 METZ Cedex 03, France
(2): Laboratoire des Essais Non-Destructifs par Ultrasons (LEND), Jijel University, 18000 Jijel, Algeria.
(*): Corresponding author Foudil MOHRI foudil.mohri@univ-lorraine.fr

ABSTRACT

The present study investigates the flexural-torsional struts buckling and beam lateral buckling analyses. In the highlight of braced structures, analytical solutions are derived for higher 3D buckling modes of simply supported struts with arbitrary cross-sections. Closed-form solutions are also investigated for lateral buckling strength of beams with doubly symmetric cross-sections. For more general cases, the finite element approach is adopted. In presence of torsion, warping is of primary importance. For this aim, 3D beams with 7 degrees of freedom (DOFs) per node are adopted in the analysis. The model is able to carry out higher buckling modes of bars under compression or lateral buckling modes of beams initially in bending. The analytical and the numerical results of the present model are compared to some available benchmark solutions of the literature and to finite element simulations of some commercial codes (Abaqus, Adina). The efficiency of the closed form solutions and the numerical approach is successfully verified. Applications of higher buckling modes in design of braced structures are considered according to Eurocode 3 code. A particular attention is pointed out to torsion and flexural-torsional buckling modes not considered in bar strength. At the end, some solutions are proposed in order to cover the full strength of columns and beams in presence of instabilities. This proposal makes steel structures more performant and attractive when effects of instabilities are limited at a minimum.

Keywords: beam; buckling; Eurocode 3; finite element; higher mode buckling, open section.

Acknowledgements: The first author (AH) received a financial support from PROFAS B+ project for a scholarship at the LEM3 laboratory, Metz, University of Lorraine. He is grateful for the ministry of the Education and Research of Algeria and France for their support. The second author (FM) is member of the National Research Agency (ANR, LabEx DAMAS).

1. Introduction and background

Thin-walled elements as beams, columns and trusses are extensively used in structural engineering field, in civil residential buildings and bridges, in aeronautics and mechanical industries. Many reasons have contributed to the increasing use of these structures. The main of them are the followings:

- The development of the industrial processes in hot and cold-formed sections permits to design any desired section shape.
- The recourse to high steel quality with increasing the yield stresses is accompanied by a drastic reduction in thickness and weight.
- Interesting solutions are now available for corrosion and connection problems based on welding, bolts or by combining the two techniques.
- The development of numerical methods and codes leads to comprehensive models for designers and engineers.

Most of thin-walled structures have open section shapes. This results in elements with low torsion strength, with one or no more axis of symmetry. The overall analysis is complex, because of the flexural-torsional coupling and the warping phenomena present with torsion. Moreover, recourse to slender elements leads to instabilities that control systematically the behaviour. This is the reason that thin-walled research field becomes attractive and is of interest to many researchers around the world. First, it is important to know that the classical buckling Euler's theory [1,2] in bending is no longer valid in the stability of thin-walled beams where 3D behaviour is present and torsion buckling modes should be present or coupled to bending modes. To our knowledge, the first works on 3D behaviour of thin-walled beams can be found in reference books [1, 3-8].

Numerous studies have investigated the stability of unrestrained beams in 3D context. Papp [9] evaluated the buckling behaviour of simply supported beams with arbitrary cross section under compressive loads. Based on the semi-analytical finite strip method, Zhang [10] investigated the stability problem of bars with open and closed cross-section under axial forces. The obtained results have been compared to finite element simulations and proven the efficiency of the model. Using the Ayrton-Perry's formula, Badari [11] investigated the lateral stability of simply supported beams under pure bending and proposed a design method in presence of initial imperfections.

Most of the previous works concerning the stability of thin-walled beam are focused in the first buckling mode in bending. They are applied to unrestrained beams and effects of bracing have not considered. The stability of thin-walled beams with restraints has been studied by several researchers [12-17]. Recently, Nguyen [18] proposed an approximative method to predict the critical buckling moment and stiffness requirements of I-section beams with discrete torsional bracing. The model is limited to simply supported beams under uniform bending moments. Comparisons with finite element shell elements have been made in the validation step. McCann [19] investigated the lateral torsional buckling capacity of beams with elastic restraints present along the beam. In this work, simply supported beams under uniform moments have been investigated and an optimization procedure for the bracing height effect is suggested. The equivalent initial imperfection method of structures sensitive to flexural and torsional buckling have been investigated in Aguero [20]. More recently, Zhang [21] studied the lateral-torsional buckling of cantilever beams in presence of lateral elastic braces. Pezeshky [22] investigated the influence of bracing position on LTB capacity of cantilever and simply supported beams and highlighted the effect of braces position on beam buckling capacity.

The behaviour of columns and beams is predominated by buckling and lateral buckling phenomena. Moreover, the buckling strength is influenced in addition to buckling by the material and geometric imperfections according to Tetmayer's approach, Engisser's theory and Aythron Perry's failure criteria [1, 23, 24]. In design, two strategies are then possible. The first is to adopt in design, efficient iterative solvers in solution of the nonlinear problem. Buckling, the geometric and material imperfections are all included in the analysis. In this case, the time consuming should be important in presence of structures with large DOFs. This procedure is commonly adopted in aeronautics field [25, 26]. The second strategy is followed in civil engineering applications as in Eurocodes 3, 4 and 5 [27-29]. In these codes, buckling loads are first obtained according to linear stability models. Analytical solutions are suggested for simple cases and recourse to numerical simulations is necessary in more general cases. In this case, buckling loads are obtained by solutions of the eigenvalue problem. In this stage, the buckling loads are evaluated in the case of ideal perfect elements. Effects of geometric and material imperfections are considered in a second stage of the design. In Eurocode 3 [27], in presence of buckling, the strength of bar with a cross section $\boldsymbol{A}$ and a yield stress $\boldsymbol{f_y}$ is affected by a reduction factor χ. This coefficient is function on bar slenderness $\bar{\lambda}$ and the geometric imperfections provided by the European curves (**a_0, a-d**). More details are given in section 4.2 of the present work.

Moreover, in engineering practices and design, the beam strength against buckling and lateral buckling is done according to the first lower buckling mode. When the buckling load is lower than the full strength, one can check that the coefficient χ is less than 0.5. The loss due to buckling should be important and can exceed 50%. The advantage of the thin-walled structures should be then less attractive.

In order to limit the buckling effect to a minimum, the value of reduction factor χ must be close to 1. This condition can only be achieved if the buckling load is as high as possible to the full strength. One possible solution to improve the beam strength against buckling and lateral buckling is to adopt higher profiles or higher steel grade. These solutions are not economic at all. Another possible and efficient strategy to limit the effects of instabilities on the strength capacity is the recourse to bracings. In this case, the buckling and lateral buckling are predominated by higher modes. Nowadays, this solution is commonly adopted in civil engineering applications as in bridge and building design but purely empirical solutions are always followed.

For this aim, we investigate in the present work an analytical and a numerical procedure for the stability of beams with open cross-section according to higher buckling modes. The finite element approach of the model is first developed in section 2. 3D beams with 7 DOFs per node are adopted in the analysis. The model is able to carry out higher buckling modes of bars under compression or lateral buckling modes of beams initially in bending. After in section 3, closed-form solutions are derived for buckling and lateral buckling. The analytical and numerical results of the present model are compared to some available benchmark solutions of the literature and to finite element simulations of the commercial codes Abaqus and Adina, in section 4. Applications of the present model in engineering construction as bridge and building design will be studied and applications to braced structures are considered for this aim at the end.

2. Finite element approach of thin-walled beam buckling

2.1 Continuum Equilibrium equations

A straight thin-walled element with slenderness ***L*** and an open cross-section ***A*** is pictured in figure 1. A direct rectangular coordinate system is chosen. Let us denote by *x* the initial longitudinal axis and by *y* and *z* the first and second principal bending axes. The origin of these axes is located at the centroid *G*. The shear point with coordinates (y_c, z_c) in *Gyz* is denoted *C*. Consider *M,* a point on the section contour with its coordinates (*y, z,* ω),ω being the sectorial co-ordinate introduced in Vlasov's model for non-uniform torsion. Hereafter, it is admitted that there are no shear deformations in the mean surface of the section and the contour of the cross-section is rigid in its own plane. This means that local and distortional deformations are not included and only slender beams are considered. Displacements and twist angle can be large but deformations are assured to be small. An elastic behaviour is then adopted. Under these conditions, displacements of a point *M* are derived from those of the shear point as:

$$u_M = u - y(v') - z(w') - \omega\theta_x'$$

$$v_M = v - e_z\theta_x \qquad w_M = w - e_y\theta_x \tag{1a-c}$$

With: $e_y = y - y_c \quad e_z = z - z_c$

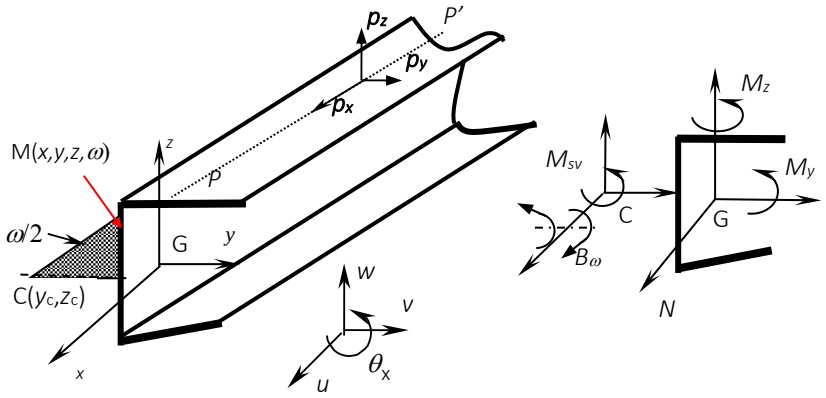

Fig.1: Open section beam with load and cross-section stress components.

The Grain's tensor strain components are the following:

$$\varepsilon_{xx} = \varepsilon - yk_z - zk_y - \omega\theta_x'' + \frac{1}{2}R^2\theta_x'^2$$

$$\varepsilon_{xy} = -\frac{1}{2}\left(e_z + \frac{\partial\omega}{\partial y}\right)\theta_x' \qquad \varepsilon_{xz} = \frac{1}{2}\left(e_y - \frac{\partial\omega}{\partial z}\right)\theta_x' \tag{2a-c}$$

In (2a):

$$\varepsilon = u' + \frac{1}{2}\left(v'^2 + w'^2\right) - (y_c w' - z_c v')\theta_x'$$

$$k_y = w'' + v'\theta_x' \qquad k_z = v'' - w'\theta_x' \tag{3a-d}$$

$$R^2 = {e_y}^2 + {e_z}^2$$

The present model is applied in the case of an elastic behaviour. In such a context and denoted by ***E*** and ***G*** the Young's and shear moduli, the relationships between the stress vector components in terms of deformation vector components are the followings in the principal axes:

$$N = \int_A E\varepsilon_{xx}dA = EA\varepsilon + \frac{1}{2}EAI_0\theta_x'^2$$

$$M_y = \int_A E\varepsilon_{xx}zdA = -EI_y\left(k_y - \beta_z\theta_x'^2\right) \tag{4a-d}$$

$$M_z = \int_A E\varepsilon_{xx}ydA = -EI_z\left(k_z - \beta_y\theta_x'^2\right)$$

$$M_{sv} = 2\int_A (G\varepsilon_{xz}(e_y - \frac{\partial\omega}{\partial z}) - G\varepsilon_{xy}(e_z - \frac{\partial\omega}{\partial y}))dA = GI_t\theta_x'$$

$$B_\omega = \int_A E\varepsilon_{xx}\omega dA = EI_\omega\left(\theta_x'' - \beta_\omega\theta_x'^2\right) \tag{4e}$$

$$M_R = EAI_0\varepsilon - 2EI_z\beta_y k_z - 2EI_y\beta_z k_y - 2EI_\omega\beta_\omega\theta_x'' + \frac{1}{2}EI_R\theta_x'^2 \tag{4f}$$

Based on stress and strain vectors components defined by:

$$\{S\}^t = \begin{Bmatrix} N & M_y & M_z & M_{sv} & B_\omega & M_R \end{Bmatrix}$$

$$\{\gamma\}^t = \begin{Bmatrix} \varepsilon & -k_y & -k_z & \theta_x' & \theta_x'' & \frac{1}{2}\theta_x'^2 \end{Bmatrix} \tag{5a,b}$$

The stress-strain relationship is written in matrix shape as:

$$\{S\} = \begin{Bmatrix} N \\ M_y \\ M_z \\ M_{sv} \\ B_\omega \\ M_R \end{Bmatrix} = \begin{bmatrix} EA & 0 & 0 & 0 & 0 & EAI_0 \\ 0 & EI_y & 0 & 0 & 0 & 2EI_y\beta_z \\ 0 & 0 & EI_z & 0 & 0 & 2EI_z\beta_y \\ 0 & 0 & 0 & GI_t & 0 & 0 \\ 0 & 0 & 0 & 0 & EI_\omega & -2EI_\omega\beta_\omega \\ EAI_0 & 2EI_y\beta_z & 2EI_z\beta_y & 0 & -2EI_\omega\beta_\omega & EI_R \end{bmatrix} \begin{Bmatrix} \varepsilon \\ -k_y \\ -k_z \\ \theta_x' \\ \theta_x'' \\ \frac{1}{2}\theta_x'^2 \end{Bmatrix} = [D]\{\gamma\} \quad (6)$$

$\{S\}$ and $\{\gamma\}$ are the stress and strain vectors. $[D]$ is the material matrix behaviour. Its terms are functions of elastic and geometric characteristics. $\boldsymbol{A}$ denotes the section area. $\boldsymbol{I_y}$ and $\boldsymbol{I_z}$ are second moments of area about *y* and *z*-axes. $\boldsymbol{I_t}$ and I_ω are respectively the St-Venant torsion and the warping constant . $\boldsymbol{I_0}$ is the polar moment of area about shear point. $\boldsymbol{\beta_y}$, $\boldsymbol{\beta_z}$ and $\boldsymbol{\beta_\omega}$ are Wagner's coefficients. $\boldsymbol{I_R}$ is the fourth moment of area about shear point. Their expressions have been shown in Mohri [31] and an efficient numerical method for their computation is described this paper. Equilibrium equations are derived from stationary condition of the total potential energy defined by:

$$\delta U - \delta W = 0 \quad (7)$$

Where $\boldsymbol{\delta U}$ and $\boldsymbol{\delta W}$ are respectively the strain energy and load work variations. The matrix formulation of these parts in terms of the displacement and their derivatives are developed separately below. Based on virtual strain deformation components and after integration over the cross-section *A*, the strain energy variation is given by:

$$\delta U = \int_L \left(N\delta\varepsilon - M_y\delta k_y - M_z\delta k_z + M_{sv}\delta\theta_x' + B_\omega\delta\theta_x'' + \frac{1}{2}M_R\delta(\theta_x')^2 \right) dx \quad (8a)$$

In matrix formulation, according to (5a, b), one can put:

$$\delta U = \int_L \{\delta\gamma\}^t\{S\}dx \quad (8b)$$

For the finite element purpose, vectors $\{\gamma\}$ and $\{S\}$ are split in terms displacement variations. According to $\{\gamma\}$ vector definition in (5a) and according to (2a) and (3) one can write:

$$\{\gamma\} = \left([H] + \frac{1}{2}[A(\theta)] - [A_c(\theta)] \right)\{\theta\} \quad (9)$$

Matrices [*H*] and [$A(\theta)$] are classical in nonlinear structural mechanics. They have been defined in Mohri [32]. The last matrix [$A_c(\theta)$] takes into account for flexural-torsional coupling. The non-vanished terms of this matrix are:

$$A_c(1,4) = y_c w' - z_c v' \qquad A_c(2,4) = v' \qquad A_c(3,4) = -w' \tag{10a-c}$$

The components of the vector $\{\theta\}$ are the following:

$$\{\theta\}^t = \{u' \quad v' \quad w' \quad \theta_x' \quad v'' \quad w'' \quad \theta_x'' \quad \theta_x\} \tag{11}$$

The variation $\{\boldsymbol{\delta\gamma}\}$ needed in the strain energy variation (8b) is:

$$\{\delta\gamma\} = \left([H] + [A(\theta)] - [A_c(\theta)] - \left[\tilde{A}(\theta)\right]\right)\{\delta\theta\} \tag{12}$$

The matrix $\left[\tilde{A}(\theta)\right]$ results from the variation of [$A_c(\theta)$]. The non-vanished terms of this matrix are:

$$\tilde{A}(1,2) = -z_c\theta_x' \quad \tilde{A}(1,3) = y_c\theta_x' \quad \tilde{A}(2,2) = \theta_x' \quad \tilde{A}(3,3) = -\theta_x' \tag{13a-c}$$

The detailed matrix formulation of strain energy variation becomes:

$$\delta U = \int_0^L \{\delta\theta\}^t \left([H] + [A(\theta)] - [A_c(\theta)] - \left[\tilde{A}(\theta)\right]\right)^t \{S\}\, dx \tag{14}$$

For the external load work variation (δW), distributed loads are applied on the cross-section contour along the line (*pp*', Fig.1). Their components $\boldsymbol{\lambda(p_x, p_y, p_z)}$ are supposed to be proportional to the load factor λ. The external load variation is then:

$$\delta W = \lambda \int_L \left(p_x \delta u_p + p_y \delta v_p + p_z \delta w_p(e_z)\right) dx \tag{15}$$

In order to take into account for second-order torsion terms of loads p_z, the expression of $\boldsymbol{w_p}$ are derived in presence of quadratic torsion terms Mohri [33]:

$$w_p(e_z) = w_p - e_z \frac{\theta_x^2}{2} \tag{16}$$

Doing variation on displacement 3D components, according to the kinematic (1a, b) and (16), the external load variation is split into two parts, written as:

$$\delta W = \delta W_c + \delta W_{nc} \tag{17a}$$

δW_c is the classical load contribution. δW_{nc} is the load height contribution of the vertical loads to the equilibrium.

$$\delta W_c = \lambda \int_L \left(p_x \delta u + p_y \delta v + p_z \delta w + m_x \delta \theta_x + m_y \delta w' + m_z \delta v' + b_\omega \delta \theta_x'\right) dx$$

$$= \lambda \int (\{\delta q\}^t \{p\} + \{\delta \theta\}^t \{m\})\, dx \qquad (17b)$$

$$\delta W_{nc} = -\lambda \int_L \left(p_z e_y \theta_x \delta \theta_x\right) dx = -\lambda \int \{\delta q\}^t [m_1]\, \{q\} dx \qquad (17c)$$

This part leads to a non-linear torsion moment proportional to ($\boldsymbol{p_z e_z \theta_x}$). In the previous equations, ($\boldsymbol{m_y = -p_x z}$, $\boldsymbol{m_z = -p_x y}$, $\boldsymbol{m_x = -p_y e_z + p_z e_y}$,and $\boldsymbol{b_\omega = -p_x \omega}$) define respectively the external bending moments, the torsion moment and the bimoment. For the matrix formulation of (δW), the additional following vectors have been used for the purpose:

$$\{q\}^t = \{u \quad v \quad w \quad \theta_x\}$$

$$\{p\}^t = \{p_x \quad p_y \quad p_z \quad m_x\} \qquad (18a\text{-}c)$$

$$\{m\}^t = \{0 \quad m_z \quad m_y \quad b_\omega \quad 0 \quad 0 \quad 0 \quad 0\}$$

$[m_1]$ is a square (4, 4) matrix. The non-vanished term of this matrix is $\boldsymbol{m_1(4,4) = p_z e_z}$

At the end, the matrix form of the external load variation is:

$$\delta W = \lambda \int_L (\{\delta q\}^t \{p\} + \{\delta \theta\}^t \{m\}) dx - \lambda \int_L \{\delta q\}^t [m_1] \{q\} dx \qquad (19)$$

The equilibrium system is carried out from (15) and (19), combined with the material behaviour (6) and (9) lead to:

$$\begin{cases} \int_L \{\delta\theta\}^t \left([H] + [A(\theta)] - [A_C(\theta)] - \left[\tilde{A}(\theta)\right]\right)^t \{S\} dx \\ -\lambda \int_L (\{\delta q\}^t \{p\} + \{\delta \theta\}^t \{m\}) dx + \lambda \int \{\delta q\}^t [m_1] \{q\} dx \qquad \forall \{\delta q\}, \{\delta \theta\} \\ \{S\} = [D] \left([H] + \frac{1}{2}[A(\theta)] - [A_C(\theta)]\right) \{\theta\} \end{cases} \qquad (20)$$

The finite element formulation of this system is investigated below.

2.2 Finite Element Approach of the equilibrium

In literature about thin-walled beams with open section, warping deformation is of primary importance. For this reason, the warping is considered as an additional independent displacement with regard to classical 3D beams. In mesh process, 3D beams elements with 14 DOFs are commonly utilized. In the present study, the beam of slenderness ***L*** is divided into some finite elements of length ***l***. Each element is modelled with 3D beams elements with two nodes and seven DOFs per node. Linear shape functions are assumed for axial displacements *u* and cubic functions for the other displacements (i.e *v*, *w*, θ_x) are used. The vectors {*q*} and $\{\theta\}$ are related to nodal variables {*r*} by:

$$\{q\} = [f(\xi)]\{r\} \quad \text{and} \quad \{\theta\} = [g(\xi)]\{r\} \tag{21a,b}$$

Where $[f(\xi)]$ is the shape functions matrix and $[g(\xi)]$ is the gradient matrix. The variation $\{\delta q\}$ and $\{\delta\theta\}$ needed in (20) are then straightforward. In the framework of finite element method, at the equilibrium, one must fulfil:

$$\begin{cases} \bigcup_e \frac{l}{2}\left(\int_{-1}^{1}[B(\theta)]^t\{S\}_e d\xi\right) - \lambda\{F\} + \lambda\{F(r)\} = 0 \\ \{S\}_e = [D]\left([B_l] + \frac{1}{2}[B_{nl}(\theta)] - [B_c(\theta)]\right)\{r\}_e \end{cases} \tag{22a,b}$$

$\bigcup_e$denotes the assembling process over basic elements. The matrices and vectors used in (22) are:

$$[B(\theta)] = [B_l] + [B_{nl}(\theta)] - [B_c(\theta)] - [\tilde{B}_c(\theta)] \tag{23a}$$

$$[B_l] = [H][g] \qquad [B_{nl}(\theta)] = [A(\theta)][g] \tag{23b,c}$$

$$[B_c(\theta)] = [A_c(\theta)][g] \qquad [\tilde{B}_c(\theta)] = \left[\tilde{A}(\theta)\right][g] \tag{23d,e}$$

$$\{F\} = \bigcup_e \frac{l}{2}\int_{-1}^{1}\{F\}_e d\xi = \bigcup_e \frac{l}{2}\int_{-1}^{1}([f]^t\{p\}_e + [g]^t\{m\}_e)d\xi \tag{24a}$$

$$\{F(r)\} = \bigcup_e \frac{l}{2}\int_{-1}^{1}\{F_1(r)\}_e d\xi = \bigcup_e \frac{l}{2}\left(\int_{-1}^{1}[f]^t[m_1][f]d\xi\right)\{r\} \tag{24b}$$

Matrices $[B_l]$ and $[B_{nl}(\theta)]$ are familiar in nonlinear analysis. The matrices $[B_c(\theta)]$ result from flexural-torsional coupling. $\{F\}$ is the classical nodal force vector. The additional force vector $\{F(r)\}$ is not constant and depends on displacements and load eccentricities. To solve the nonlinear problem (22), the classical incremental-iterative Newton-Raphson procedure is followed. With this aim in view, we have to compute the tangent stiffness matrix. If the unknowns of the problem (22) are sought in the form:

$$\{r\} = \{r_0\} + \{\Delta r\} \qquad \{S\} = \{S_0\} + \{\Delta S\} \qquad \lambda = \lambda_0 + \Delta\lambda \tag{25a-c}$$

And given an initial guess of the solution ($\{r_0\}$, $\{S_0\}$, λ_0), the increments of the problem ($\{\Delta r\}$, $\{\Delta S\}$, $\Delta\lambda$) fulfil the following conditions:

$$\bigcup_e \frac{l}{2}\int_{-1}^{1}([B(\theta_0)]^t\{\Delta S\} + [\Delta B(\theta)]^t\{S_0\})\,d\xi - \Delta\lambda\{\mathrm{F}\} + \Delta(\lambda\{F(r)\}) = 0 \tag{26a,b}$$

with $\{\Delta S\} = [D]\{\Delta\gamma\} = [D][B(\theta)]\{\Delta r\}$

Due to coupling terms involved in matrix $[B(\theta)]$, the increments $[\Delta B(\theta)]$ in (26a) is not straightforward and must be computed with more caution. According to (26b), one can write for the geometric stiffness matrix part.

$$[\Delta B(\theta_0)]^t\{\Delta S\} = [B(\theta_0)]^t\,[D][B(\theta_0)]\{\Delta r\} = \left[K_g\right]\{\Delta r\}$$

The second term leads to the initial stress stiffness matrix. Following the procedure adopted in Mohri [32], one arrives to:

$$[\Delta B(\theta)]^t\{S_0\} = [g]^t\left([\bar{S}_0] - \left[\bar{\bar{S}}_0\right] - \left[\bar{\bar{S}}_0\right]^t\right)[g]\{\Delta r\} = [g]^t[S_0][g]\{\Delta r\} = \left[K_{s_0}\right]\{\Delta r\} \tag{27}$$

In (27) we have put: $[S_0] = [\bar{S}_0] - \left[\bar{\bar{S}}_0\right] - \left[\bar{\bar{S}}_0\right]^t$.

The non-vanished terms of the initial stress matrices are the following.

$$\bar{S}_0(2,2) = \bar{S}_0(3,3) = N_0\ ,\quad \bar{S}_0(4,4) = M_{R0} \tag{28a, b}$$

$$\bar{\bar{S}}_0(4,2) = -N_0 z_c + M_{y0}\,, \quad \bar{\bar{S}}_0(4,3) = N_0 y_c - M_{z0} \tag{28c, d}$$

Moreover, in the present study, the applied load displacement dependent. Remind that load contribution has been derived in (24) by its classical component {*F*} (24a) is displacement dependent part {*F*(*r*)} (24b). So:

$$\Delta\lambda\{F\} - \Delta(\lambda\{F(\mathrm{r})\}) = \Delta\lambda(\{F\} - \{F(r_0)\}) - \lambda_0\{F(\Delta r)\} \tag{29a}$$

with: $\{F(r_0)\} = \cup_e \frac{l}{2}\left(\int_{-1}^{1}[f]^t[m_1][f]\,d\xi\right)\{r_0\}$

$$\{F(\Delta r)\} = \cup_e \frac{l}{2}\left(\int_{-1}^{1}[f]^t[m_1][f]\,d\xi\right)\{\Delta r\} = [K_F]\{\Delta r\} \tag{29b,c}$$

Finally, the global matrix form of the incremental problem (26) can be written as:

$$[K_t]\{\Delta r\} = \Delta\lambda\{F\} \tag{30a}$$

The tangent stiffness matrix [$\boldsymbol{K_t}$] is given by

$$[K_t] = \left[K_g\right] + \left[K_{S_0}\right] + [K_F] \tag{30b}$$

With:

$$\left[K_g\right] = \cup_e \frac{l}{2}\left(\int_{-1}^{1}[B(\theta_0)]^t[D][B(\theta_0)]\,d\xi\right)$$

$$\left[K_{S_0}\right] = \cup_e \frac{l}{2}\left(\int_{-1}^{1}[g]^t[S(\theta_0)][g]\,d\xi\right) \tag{30c-e}$$

$$[K_F] = \lambda_0\left\{\cup_e \frac{l}{2}\left(\int_{-1}^{1}[f]^t[m_1][f]\,d\xi\right)\right\}$$

[K_g] is the geometric stiffness matrix and [K_{S0}] is the initial stress stiffness matrix. The matrix **[$\boldsymbol{K_F}$]** is the contribution of eccentric loads to the stiffness. The load height parameter is present in this matrix. This part is not classical is structural mechanics where the applied forces are constant and independent on displacements. In our case, it leads to load height effects in stability. The system (30) can be solved with the help of the iterative methods and the load displacements equilibrium

curves can be obtained. This task has been done in more general case and in presence of large or finite torsion amplitudes [32, 34]. Moreover, in presence of instabilities, the buckling loads can be researched from the singularities of the tangent matrix [$\boldsymbol{K_t}$]. When this matrix is sought according to the geometric and initial stress parts, the buckling loads are carried out according to the solution of the eigenvalue problem given by:

$$\left(\left[K_g\right] - \lambda_0\left(\left[K_{s_0}\right] - \left[K_F\right]\right)\right)\{r\} = \{0\} \tag{31}$$

λ_0 and $\{r\}$ and the buckling loads and the related eigenmodes. They are carried out according to an efficient solver of the eigenvalue problem. In Abaqus [30], Lanczos and subspace methods are possible. In the present model, an efficient eigenvalue problem solver present in Matlab [35] is adopted. The present finite element model is implemented in this code. It is referenced B3Dw in the application part.

3. Analytical solutions attempt for higher buckling and lateral buckling modes for unrestrained beams

In the finite element approach investigated previously, 3D load cases are possible. Moreover, in presence of buckling and lateral buckling instabilities, loads of interest in the study are the axial and the vertical loads ($\boldsymbol{p_x}$ and $\boldsymbol{p_z}$) that cause respectively in the beam the axial stress forces $\boldsymbol{N}$ and bending moment $\boldsymbol{M_y}$ about the strong axis y. In this context, adapting the strain energy presented by Mohri [33], for an unrestrained beam with arbitrary open cross-sections under axial and bending loads, the strain energy of the beam in presence of buckling and lateral buckling stabilities is given by:

$$\boldsymbol{U} = \frac{1}{2}\int_0^L \left(EAu'^2 + EI_z v''^2 + EI_y w''^2 + EI_\omega \theta_x''^2\right)dx + \frac{1}{2}\int_0^L \left(GI_t \theta_x'^2\right)dx$$

$$+ \int_0^L N\left(\frac{1}{2}v'^2 + \frac{1}{2}w'^2 + \frac{I_0}{2}\theta_x'^2 + z_c v'\theta_x' - y_c w'\theta_x'\right)dx + \int_0^L M_y\left(v''\theta_x + \beta_z \theta_x'^2\right)dx \qquad (32)$$

The work done by the uniformly distributed loads $\boldsymbol{p_x}$ and $\boldsymbol{p_z}$ is

$$\boldsymbol{W} = \int_0^L \left(p_x u + p_z(w + \frac{1}{2}e_z\theta_x^2\right)dx \qquad (33)$$

At equilibrium under static loads, one must fulfil the condition ($\delta\boldsymbol{\Pi}$=0). System (32) and (33) can be applied in behaviour and in stability analyses. Moreover, for the buckling study in presence of a constant compressive load $\boldsymbol{P}$, the terms of interest are reduced to:

$$\boldsymbol{\Pi} = \frac{1}{2}\int_0^L \left(EI_z v''^2 + EI_y w''^2 + GI_t \theta_x'^2 + EI_\omega \theta_x''^2\right)dx$$

$$- P\int_0^L \left(\frac{1}{2}v'^2 + \frac{1}{2}w'^2 + \frac{I_0}{2}\theta_x'^2 + z_c v'\theta_x' - y_c w'\theta_x'\right)dx \qquad (34)$$

In lateral buckling analysis in presence of initial bending load $\boldsymbol{p_z}$, the potential is given by:

$$\boldsymbol{\Pi} = \frac{1}{2}\int_0^L \left(EI_z v''^2 + GI_t \theta_x'^2 + EI_\omega \theta_x''^2\right)dx + \int_0^L M_y\left(v''\theta_x + \beta_z\theta_x'^2\right)dx + \frac{1}{2}\int_0^L p_z e_z \theta_x^2 dx \qquad (35)$$

Let us remind that in lateral buckling analysis (35), the study includes in addition to bending stiffness about the weak axis and torsion and warping stiffness, the contribution of load height position from the shear point ($\boldsymbol{e_z}$) and the Wagner's coefficient ($\boldsymbol{\beta_z}$). To get analytical solutions of these problems (34, 35), Galerkin's or Rayleigh-Ritz methods are possible and the resulting algebraic system must be solved using singularity condition. Closed form solutions for higher buckling and lateral buckling loads are derived according to a priori known buckling modes. In the case of simply supported beams, the bending displacement components $v(x)$, $w(x)$ and the torsion angle $\theta(x)$ are approximated by the following shape modes:

$$v(x) = v_k \, sin\left(\frac{k\pi x}{L}\right) \;,\; w(x) = w_k \sin\left(\frac{k\pi x}{L}\right) \quad \text{and} \quad \theta(x) = \theta_k \sin\left(\frac{k\pi x}{L}\right) \quad k=1...n \qquad \text{(36a-c)}$$

Where v_k, w_k and θ_k are the undetermined amplitudes and k is the buckling mode number.

3.1 Analytical solution for higher buckling modes

Substitution of the assumed deflection function (36a-c) into the total potential energy expression (34) and after integration and needed simplifications, one gets the equilibrium system for a mode k given in matrix system by:

$$\begin{bmatrix} P_z(k) - P & 0 & -z_c P \\ 0 & P_y(k) - P & y_c P \\ -z_c P & y_c P & I_0(P_\theta(k) - P) \end{bmatrix} \begin{Bmatrix} v_k \\ w_k \\ \theta_k \end{Bmatrix} = \begin{Bmatrix} 0 \\ 0 \\ 0 \end{Bmatrix} \qquad (37)$$

In this system, $P_y(k)$ and $P_z(k)$ are the buckling loads in pure bending about the strong and the weak axes. $P_\theta(k)$ is the pure torsion buckling load. They are defined by:

$$P_z(k) = \frac{k^2\pi^2 EI_z}{L^2} \;, \qquad P_y(k) = \frac{k^2\pi^2 EI_y}{L^2} \qquad \text{and} \quad P_\theta(k) = \frac{1}{I_0}\left(\frac{k^2\pi^2 EI_\omega}{L^2} + GI_t\right) \qquad \text{(38a-c)}$$

The buckling loads can be obtained from the nontrivial solutions of Eq. (37). Closed form solutions are possible for usual cross sections as doubly symmetric or singly symmetric shapes. However,

finding analytical solutions for an arbitrary cross section is a complicated task. Moreover, a semi-analytical procedure is attempted below.

For doubly cross sections ($y_c = z_c = 0$), the equation (37) is fully uncoupled. The buckling loads for the *k*-mode (*k=1… n)* are given in (38). The bar can buckle in classical pure bending (Euler's buckling) or in pure torsional buckling mode. One can easily obtain the classical buckling loads used in design by putting ***k*=1**. In this case, since the buckling load P_y is the highest, one understands easily that the buckling design load is the minimum of P_z and P_θ.

Moreover, equations (37) permit to get the buckling loads of a braced beam in terms of the number of the braces. According to these solutions, in presence of n_y, n_z and n_θ braces equally positioned along the beam in the direction *y*, *z* and in torsion, higher buckling loads happen, given by:

$$P_z = (n_z+1)^2\frac{\pi^2 EI_z}{L^2}\ ,P_y = (n_y+1)^2\frac{\pi^2 EI_y}{L^2}\ \text{ and }\ P_\theta = \frac{1}{I_0}\left((n_\theta+1)^2\frac{\pi^2 EI_\omega}{L^2}+GI_t\right) \quad \text{(39a-c)}$$

Since the number of braces should be arbitrary, the 3 buckling loads should be then important in the design step of braced columns.

If there is only one axis of symmetry, say the *y*-axis, then shear centre lies on the y-axis and the shear centre z_c=0 (as in channel section). Hence, in this case, the bar can buckle in two possible buckling modes namely pure bending in the ***z***-axis or flexural-torsional buckling modes. Solutions of system (37) lead to the following buckling loads given by

$$P_{cr} = min\left(P_z(k), P_{y\theta}(k)\right) \quad \text{(40a)}$$

$P_z(k)$ is the pure bending load defined in (38a). $P_{y\theta}(k)$ are the flexural-torsional buckling loads defined by

$$P_{y\theta}(k) = \frac{P_y(k)+P_\theta(k) \pm \sqrt{\left(P_y(k)+P_\theta(k)\right)^2 - 4a_c\,P_y(k)P_\theta(k)}}{2a_c}$$

With: $\quad a_c = \left(1-\frac{y_c^2}{I_0}\right)$ (40b-c)

If the symmetry axis is the z-axis (as in Tee sections, y_c =0), similar closed-form solutions for the buckling loads are possible. The buckling loads are given by:

$$P_{cr} = min\big(P_y(k), P_{z\theta}(k)\big) \tag{41a}$$

$P_y(k)$ is the pure bending load defined in (38b). $P_{z\theta}(k)$ are the flexural-torsional buckling loads given by

$$P_{z\theta}(k) = \frac{P_z(k) + P_\theta(k) \pm \sqrt{\big(P_z(k) + P_\theta(k)\big)^2 - 4a_t\, P_z(k)P_\theta(k)}}{2a_t}$$

With: $a_t = \left(1 - \frac{z_c^2}{I_0}\right)$ (41b-c)

It is important to mention that for k=1, one obtains the smallest of each buckling mode used in classical design methods**.** The similar closed form solutions have been carried out in Mohri [31]. Let us remind, that according to (40a, b) or (41a, b), three solutions are possible for the buckling loads: one in pure bending and two others are flexural-torsional. All the three solutions are necessary for higher modes analyses purpose.

If there is no axis of symmetry ($y_c \neq 0$; $z_c \neq 0$), from the system (37), closed-form solutions are not possible but only semi-analytical solutions are possible. They can be obtained from solution of the following cubic equation obtained from system (37):

$$(P_z(k) - P)\big(P_y(k) - P\big)(P_\theta(k) - P) - P^2(P_z(k) - P)\frac{y_c^2}{I_0} - P^2\big(P_y(k) - P\big)\frac{z_c^2}{I_0} = 0 \tag{42}$$

In this case, all the buckling modes are fully coupled (flexural torsional modes). For a given mode k, 3 solutions are possible. They are all lower than the uncoupled buckling loads $P_y(k)$, $P_z(k)$ and $P_\theta(k)$. This is the reason why solutions of (42) are more important in design. These 3 solutions are all necessary in the context of higher mode analyses. In the present contribution, solutions of (42) are implemented on Matlab code [35] for any mode ***k***. Let us remind that in the literature, the available solutions for higher buckling loads exist only in the case of pure bending (the classical Euler's

buckling theory [1-2]). The closed-form solutions derived here for flexural torsional buckling are original.

3.2 Analytical solution attempts of higher modes for beam lateral buckling

In the present study, we limit the study to the case of simply supported beams with doubly symmetric I-beams under distributed and concentrated load applied at mid-span (Fig.2a, b). These load cases are the most important in engineering design applications. Effect of load position (Fig.2c) is taken into account in the analysis. Closed form solutions for higher lateral buckling moment are carried out according to the Ritz or Galerkin's methods. For this purpose, the potential derived in (35) and mode shapes (36a, c) are used.

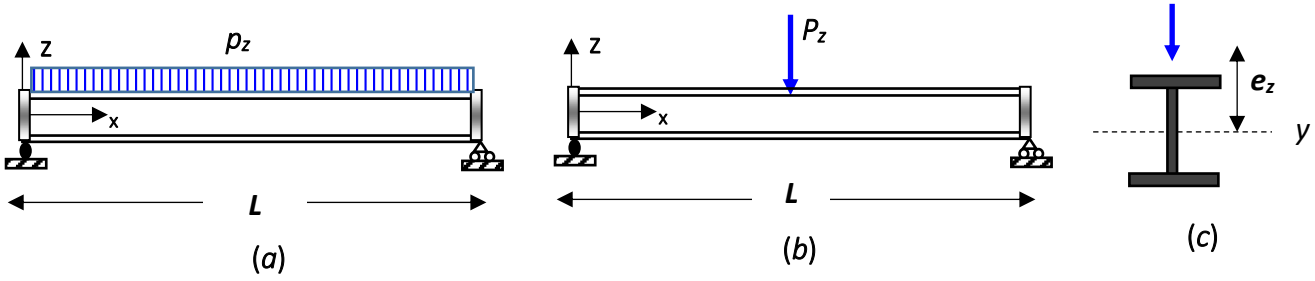

Fig.2: Simply supported beam with doubly symmetric section subjected to uniformly distributed **(*a*)** and concentrated loads **(*b*)** with load position **(*c*)**.

In the case of uniformly distributed load p_z (Fig.2a), the bending moment is the following:

$$M_y(x) = \frac{4M_0}{L^2}x(L-x) \qquad \text{with } M_0 = \frac{p_z L^2}{8} \tag{43}$$

In presence of a concentrated load P_z applied at $L/2$ (Fig.2b), the bending moment expression is

$$M_y(x) = \frac{2M_0}{L}\,x \qquad 0 \le x \le \frac{L}{2}$$

$$M_y(x) = \frac{2M_0}{L}\,(L-x) \qquad \frac{L}{2} \le x \le L \qquad \text{with } M_0 = \frac{P_z L}{4} \tag{44}$$

For the uniformly distributed load, the mode shapes (36a, c) and equation (43) are used. While in the concentrated load case, mode shapes (36a, c) combined with equations (44) are necessary. These relationships are respectively included in the potential (35) and after needed integration, the buckling moments of the beam are obtained for each load case. Since the Wagner's coefficient (β_z) vanishes, the new expression for the mode number k, denoted $M_{cr}(k)$ is the following.

$$M_{cr}(k) = C_1(k)P_z(k)\left[C_2(k)e_z + \sqrt{(C_2(k)e_z)^2 + \frac{I_\omega}{I_z}\left(1 + \frac{GI_tL^2}{k^2\pi^2EI_\omega}\right)}\right] \quad (45)$$

Where $P_z(k)$ denotes the Euler's buckling load defined in (38). The coefficients $C_1(k)$ and $C_2(k)$ are function on load case. For distributed load:

$$C_1(k) = \frac{3k^2\pi^2}{2(k^2\pi^2+3)} \qquad C_2(k) = \frac{6}{k^2\pi^2+3} \quad (46)$$

In the case of concentrated load, these terms depend on mode number.

- For odd number mode (k=1, 3, 5… : symmetric modes):

$$C_1 = \frac{2k^2\pi^2}{(k^2\pi^2+4)} \qquad C_2 = \frac{8}{k^2\pi^2+4} \quad (47)$$

- For even number mode (k=2, 4, 6.. : anti-symmetric modes):

$$C_1 = 2 \qquad C_2 = 0 \quad (48)$$

The relationship (45) is more general and permits to obtain the lateral buckling moment for higher modes. Using this expression, the classical compact equation of mode 1, adopted in lateral buckling analysis is straightforward, by putting (***k*=1**). One finds:

$$M_{cr} = C_1P_z\left[C_2e_z + \sqrt{(C_2e_z)^2 + \frac{I_\omega}{I_z}\left(1 + \frac{GI_tL^2}{\pi^2EI_\omega}\right)}\right] \quad (49)$$

According to (46) and (47), one gets respectively for the first mode number (k=1: C_1=1.15, C_2=0.46) in the uniformly load case and (k=1: C_1=1.42, C_2=0.58) for the concentrated load case. These values are close to the improved values obtained in Mohri [33] and adopted in EC3. In the present study,

the higher lateral buckling modes (*k*) are researched, all terms depend on the mode number ***k***. The mode number ***k*** is present in the Euler's buckling load $\boldsymbol{P_z}$, in the coefficients $\boldsymbol{C_1}$ and $\boldsymbol{C_2}$ and in the St-Venant warping ratio ($\frac{GI_tL^2}{k^2\pi^2EI_\omega}$). Again, the lateral buckling moments (45) derived in the present work in terms of load height parameter and higher mode *k* are then original.

In the present study, the finite element model and the analytical solutions derived for higher modes of column buckling and beam lateral buckling will be validated hereafter according to benchmark solutions and to other finite element simulations carried out on Abaqus and Adina codes [30, 36]. Applications of higher modes in design are presented at the end (**section 5**), where effects of bracing on column buckling and beam lateral buckling strength capacities are considered according to the Eurocode 3 design code. Different cross sections and boundary conditions are studied for the purpose.

4. Comparison examples and numerical simulations

This section is divided into two main parts. Firstly, column buckling under compressive loads is investigated (section 4.1), while the beam lateral buckling is provided in section 4.2. For each example, analytical and numerical solutions of higher buckling modes are found and compared.

4.1 Buckling Analysis

In order to evaluate the validity of proposed closed solution and the present 3D beam finite element model (called B3Dw), bars with different slenderness are considered. Different cross sections are also considered: singly symmetric and arbitrary sections. In all the study, steel material is adopted with the following elastic constants: Young's and moduli ($\boldsymbol{E}$ *=210*, $\boldsymbol{G}$ *= 80.77 GPa*). For all the studied bars, two scenarios are analysed (1): the variation of first buckling load in terms of the bars slenderness, (2): higher buckling analysis of the bar for a fixed length. When possible, the present analytic and numeric solutions are compared to benchmark solutions or to simulations of the commercial software Abaqus [30] in which B31OS beam element with generalized sections have been used. Effect of meshing on solution accuracy has been studied initially. The number of elements has been increased until the solution becomes insensitive to mesh. In the present study, since we have concerned by higher buckling modes of beams with variable slenderness, the optimal element length is 10 cm. This means that in presence of a beam with 4 m, 40 elements (287 DOFs) are needed.

The present study is concerned with the overall buckling problem. For this aim, only slender beams are considered in the study where this assumption is checked [37-39]. Local buckling is ignored. For this topic, one can see the rich available literature quoted in [40-42].

Example 1: Buckling of bar with singly symmetric cross sections about the y-axis

In this example, a singly symmetric cross-section about the y-axis is analysed (namely channel section). The dimensions of the section are presented in Fig. 3. The geometric parameters of this section are calculated according to Mohri [31]. Table 1 gives a comparison of the predicted buckling loads of the bar when the slenderness *L* varies from 2 to 8 m. The analytical and the numerical solutions are presented. The analytical solutions for this case are predicted based on equations (40). These solutions are possible from the uncoupled buckling loads of the cross section reproduced in the first three columns of table 1 for clarity. The numerical results are related to the beam finite element of the present model (B3Dw) and Abaqus element (B31OS). It is observed that the buckling loads decrease when the length increases. The results also indicate that the flexural-torsional buckling is the dominant buckling modes when the length *L*<3m. The Euler's bending buckling load is present for lengths higher than 3m. From this, it can be concluded that the buckling behaviour of C-section is dependent on the beam length. One observes a good agreement between the present analytic and finite element results and Abaqus simulations. The error between B3Dw and Abaqus is not higher than 1%. In order to assess the effect of higher buckling modes, the same channel section bar is reconsidered with span fixed to *L* =4 m and the first four buckling modes are researched. Comparisons between the predictions of analytic, B3Dw and Abaqus are provided in Table 2. For this length, the modes 1 and 4 are pure bending (PB), while the other modes (2 and 3) are flexural torsional (FT). The mode shapes of this case are depicted in Fig.A1 of the appendix.

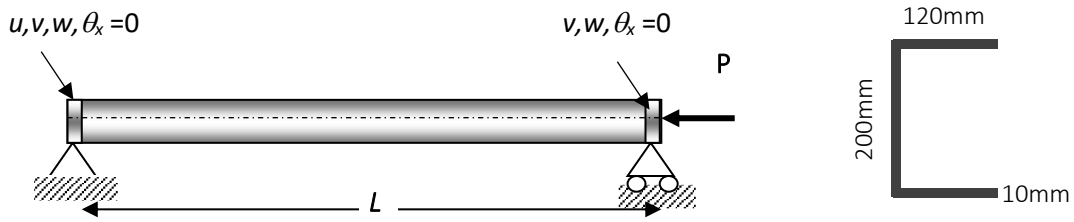

Fig.3: Bar with channel section: boundary conditions, load application and cross-section dimensions.

L	P_y	P_z	P_θ	$P_{y\theta}$	$P_{cr,th}$	Present	Abaqus	Mode	Error
(m)			(kN)		min(P_z,$P_{y\theta}$)	B3Dw	B31OS	type	(%)
2	13717,27	3095,90	2269,38	**2104,77**	2104,77	2104,78	2117,00	**FT**	0,58
3	6 096,56	1375,96	1470,89	**1314,88**	1314,88	1314,89	1322,00	**FT**	0,54
4	3 429,32	**773,98**	1191,42	1009,65	773,98	773,98	772,77	**PB**	0,16
5	2 194,76	**495,34**	1062,07	838,44	495,34	495,35	494,85	**PB**	0,10
6	1 524,14	**343,99**	991,80	716,99	343,99	343,99	343,75	**PB**	0,07
7	1 119,78	**252,73**	949,43	619,11	252,73	252,73	252,60	**PB**	0,05
8	857,33	**193,49**	921,94	536,04	193,49	193,50	193,42	**PB**	0,04

Table 1: Channel section: numerical and analytical buckling loads variation versus the length L. (FT: Flexural-Torsional mode, PB: Pure Bending mode).

Higher buckling loads ***L***=4m					
Mode number	P_{cr} (Theory, kN)	Present B3Dw	Abaqus B31OS	Mode type	Error %
1	773,98	773,98	772,77	**PB**	0,16
2	1009,34	1009,65	1014,60	**FT**	0,49
3	2104,13	2104,78	2117,00	**FT**	0,58
4	3095,91	3095,92	3076,40	**PB**	0,63

Table 2: Channel section, numerical and analytical buckling loads of the first four modes. (**FT**: Flexural-Torsional mode, **PB:** Pure Bending mode).

Example 2: Buckling of bar with singly symmetric cross sections about the z-axis

The present example is aimed to investigate the buckling behaviour of column with singly symmetric about the z-z axis. Two sections are studied. The first is a mono-symmetric I-section and the second is a Tee section. Their dimensions are summarized in Fig 4. For the both sections, the buckling load variation is analysed with length ***L*** varied from 2 until 8m. Table 3a compares the buckling loads of the singly-symmetric I-section. Closed form solutions given in (41) are computed and compared to finite element models simulations. In the interests of clarity, the uncoupled buckling loads of these cross sections are reproduced in the first three columns. The same procedure is followed for the Tee cross section and results are summarized in Table 4a. For the two sections, it is observed that the flexural-torsional buckling mode controls the bar strength for all the considered slenderness. The results of the present model are in excellent agreement with Abaqus simulations. The maximum error does not exceed 1.20%.

The effect of higher buckling modes is also analysed, for this aim, we consider once again the both sections, but now the length is fixed to ***L***=4m and the first four buckling modes are sough. The resulting buckling loads are illustrated in Table 3b for the singly I section and Table 4b for the Tee section. It can be seen that all the higher modes are flexural torsional and no bending mode is present in the first four modes. Again, in higher mode analysis, the beam resistance depends only on flexural torsional modes. As for channel section, the mode shapes of the Tee section are presented in Fig. A2 of the Appendix.

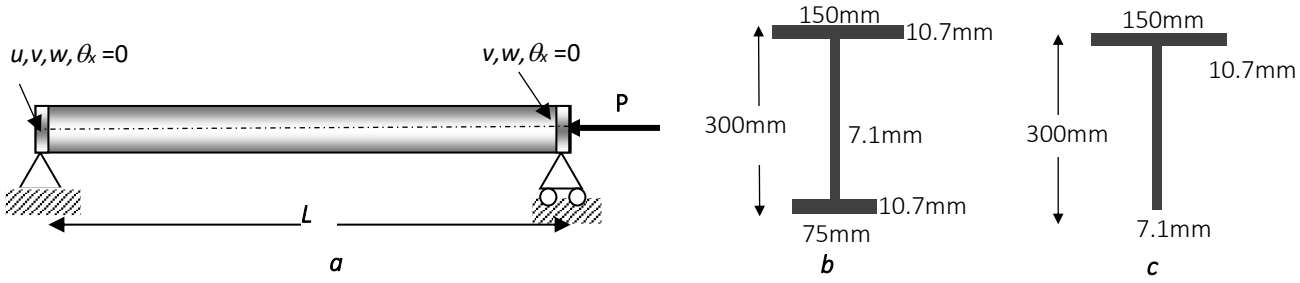

Fig.4: bar with singly symmetric I and Tee cross sections, (a): boundary conditions and load application, (b): singly-symmetric I section dimensions and (c): Tee section dimensions.

L	P_y	P_z	P_θ	$P_{z\theta}$	$P_{cr,th}$	Present	Abaqus	Mode	Error
(m)			(kN)		min(P_y, $P_{z\theta}$)	B3Dw	B31OS	type	(%)
2	31150,40	1758,56	3280,87	**1149,96**	1149,96	1149,96	1152,70	**FT**	0,24
3	13844,62	781,58	2185,65	**577,88**	577,88	577,88	578,33	**FT**	0,08
4	7787,60	439,64	1802,32	**354,51**	354,51	354,51	354,63	**FT**	0,03
5	4984,06	281,37	1624,89	**240,42**	240,42	240,42	240,46	**FT**	0,01
6	3461,16	195,40	1528,52	**173,59**	173,59	173,59	173,59	**FT**	0,01
7	2542,89	143,56	1470,40	**130,99**	130,99	130,99	131,00	**FT**	0,01
8	1946,90	109,91	1432,68	**102,21**	102,21	102,21	102,21	**FT**	0,01

Table 3a: Singly-symmetric I-section, numerical and analytical buckling loads variation versus length L. (FT: Flexural-Torsional mode).

Higher buckling loads ***L***=4m					
Mode number	P_{cr} (Theory, kN)	Present B3Dw	Abaqus B31OS	Mode type	Error %
1	354,51	354,51	354,63	**FT**	0, 03
2	1149,96	1149,96	1152,70	**FT**	0,23
3	2354,08	2354,10	2369,20	**FT**	0,63
4	4004,48	4004,50	4053,80	**FT**	1,20

Table 3b: Singly-symmetric I-section, numerical and analytical solutions buckling loads of the first four modes.

L	P_y	P_z	P_θ	$P_{z\theta}$	$P_{cr,th}$	Present	Abaqus	Mode	Error
(m)		(kN)			min(P_y,$P_{z\theta}$)	B3Dw	B31OS	type	(%)
2	17934,87	1563,79	459,95	**403,15**	403,15	403,15	402,99	**FT**	0,04
3	7971,05	695,02	447,52	**328,30**	328,30	328,30	328,07	**FT**	0,07
4	4483,72	390,95	443,17	**253,51**	253,51	253,51	253,31	**FT**	0,08
5	2869,58	250,21	441,16	**191,03**	191,03	191,03	190,90	**FT**	0,07
6	1992,76	173,75	440,06	**144,90**	144,90	144,90	144,82	**FT**	0,06
7	1464,07	127,66	439,40	**112,09**	112,09	112,09	112,04	**FT**	0,04
8	1120,93	97,74	438,98	**88,64**	88,64	88,64	88,61	**FT**	0,03

Table 4a: Tee section, numerical and analytical buckling loads variation versus length L, (FT: Flexural-Torsional mode).

Higher buckling loads ***L***=4m					
Mode number	P_{cr} (Theory, kN)	Present B3Dw	Abaqus B31OS	Mode type	Error %
1	253,51	253,51	253,31	FT	0.08
2	403,14	403,15	402,99	FT	0.04
3	459,86	459,87	460,10	FT	0.05
4	508,78	508,78	510,02	FT	0.24

Table 4b: Tee section, numerical and analytical solutions buckling loads of the first four modes.

Example 3: Buckling analysis of beam with arbitrary cross sections

This arbitrary cross section has been studied by Papp [9]. The properties of this cross-section are produced in figure 5. In the present study, the buckling loads have been computed in terms of the slenderness *L* varied from 2 to 8m. The analytical and the numerical buckling loads are summarized in Table 5. The present model is compared to Abaqus simulations. Since the cross section is arbitrary, the analytical solutions of the buckling load are not straightforward. In the present model, they have been obtained numerically by solutions of Eq (42). For this aim, the uncoupled buckling loads P_y, P_z and P_θ are needed. They are given for the purpose in table 5. The analytical results are enclosed in column 5 for comparison. The analytical and the numerical results of the present model concord well. Moreover, Papp [9] considered only the slenderness ***L=4m*** and obtained a buckling load $\boldsymbol{P_{cr}=299.16}$ *kN*. This result is in good agreement with our model where $\boldsymbol{P_{cr}=299, 07}$ kN is obtained numerically and 299.06 analytically. Let us remind that for this section, all the buckling modes are flexural-torsional buckling. Displacements *v, w* and the torsion angle θ_x are present in all modes.

For this section effects of higher buckling modes are considered for the beam length *L* = 4 m. For this length, the first four buckling loads have been computed. They are presented in Table 6. It is confirmed that all the higher modes are also Flexural-Torsional (FT). A good agreement between the different solutions is remarked. The error does not exceed 1%. The first four buckling mode shapes of this section are given in Fig. A3 of the appendix.

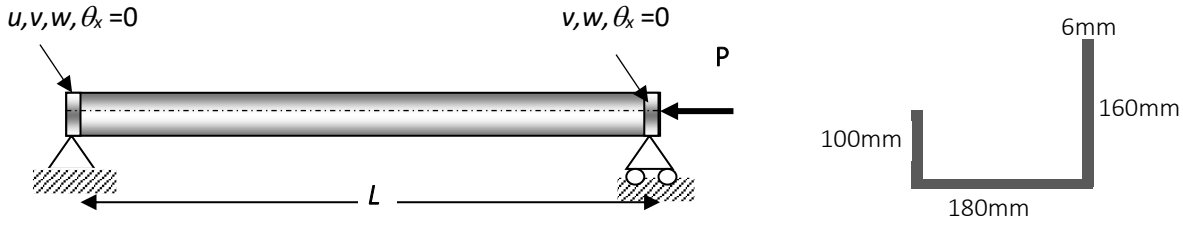

Fig.5: bar with arbitrary section, boundary conditions, load application and cross-section dimensions.

L	P_y	P_z	P_θ	$P_{cr,th}$	Present	Abaqus	Mode	Error
(m)		(*kN*)		(Eq,42)	B3Dw	B31OS	type	(%)
2	2429,11	7575,41	808,82	764,32	764,36	771,94	**FT**	0,98
3	1079,60	3366,85	452,85	421,51	421,53	421,27	**FT**	0,06
4	607,28	1893,85	328,27	299,06	299,07	299,13	**FT**	0,02
5	388,66	1212,07	270,60	239,68	239,69	239,35	**FT**	0,14
6	269,90	841,71	239,27	204,52	204,52	204,20	**FT**	0,16
7	198,29	618,40	220,39	179,58	179,57	179,29	**FT**	0,16
8	151,82	473,46	208,13	149,95	149,89	149,89	**FT**	0,00

Table 5: Arbitrary section, numerical and analytical buckling loads variation versus length *L*. (FT: Flexural-Torsional mode).

Higher buckling loads ***L***=4m					
Mode number	P_{cr} (Theory, kN)	Present B3Dw	Abaqus B31OS	Mode type	Error %
1	299,06	299,07	299,13	FT	0.02
2	608,91	608,65	607,55	FT	0.18
3	764,32	764,37	765,22	FT	0.11
4	1531,36	1531,61	1534,80	FT	0.21

Table 6: Arbitrary section, numerical and analytical buckling loads of the first four modes. (FT: Flexural-Torsional mode)

4.2 Lateral buckling beam analysis

In section 3-2, closed form solutions have been attempted for lateral buckling of beam with doubly symmetric cross-sections under uniformly and concentrated loads. Load height parameter is taken into consideration. These solutions are able to find higher lateral buckling moments of the beam. These solutions are checked below following the same procedure as for buckling analysis considered previously. For this aim, the analytical solutions for each load case are computed and compared to the numerical simulations resulting from the finite element approach of the present model (B3Dw), from beam elements of Abaqus and Adina codes. The same material data of the steel is used. In the study, the cross-section IPE300 ($\boldsymbol{h}$=300, $\boldsymbol{b}$=150, $\boldsymbol{t_f}$ =10.7, $\boldsymbol{t_w}$=7.1 mm) is adopted. In a first stage, the lower buckling moment variation in terms of the slenderness $\boldsymbol{L}$ and the load height position is studied. Load position of the load is on the Shear Centre point (**SC**), on Bottom Flange (**BF**) or Top Flange (**TF**). The study is followed by consideration of the effects of higher modes and loading applications for a fixed slenderness.

The variation of the lower buckling moment ($\boldsymbol{k}$=1) in terms of the slenderness $\boldsymbol{L}$ varied from 4 to 8 m is depicted in Fig. 7 for the 3 load positions. The uniform load case is in Fig.7a and the concentrated load case follows in Fig. 7b. One remarks that for these load cases, the lateral buckling strength is best when load is on (BF) and the lower values are obtained when the loads are on (TF) position.

For each case and load position, a good agreement between the proposed analytical and numerical solutions of the present model with the Abaqus beam element. This is true for the two load cases and the three load positions. Moreover, Adina's simulations overestimate the lateral buckling strength when load is on bottom flange. The discrepancy is not important and decreases with the slenderness.

For higher lateral buckling modes studies, the beam length ***L*=6m** is selected in the analysis and the first four modes of the beam are researched in terms of load positions for the two load cases. Results of the uniformly load case are presented in Fig.8 a-c, followed by the concentrated load case in fig. 9a-c. In the ordinate, the non-dimensional buckling moment $M_{cr}(k)/M_{cr,ref}$ are reported. For each load position, $M_{cr}(k)$ denotes the buckling moment of mode k and $M_{cr,ref}$ is the buckling moment of the first mode for load position on SC. These values are respectively $M_{cr,ref}$ =94.23 kNm for the uniformly load case and $M_{cr,ref}$ =113.22 kNm for the concentrated load case. One can check again that:

- All the results have the same tendency in terms of the mode number and load position. A good agreement is observed between the present model (theory and B3Dw) and the other finite elements codes.

- A discrepancy is remarked with Adina code for the uniformly distributed load case when loadings on top or bottom flange. This finding has been also reported in [43]. The maximum error of 8% is obtained for the beam under distributed load for load position on top flange (Fig.8b).
- One remarks that the analytic solutions are accurate for the both load cases and for load position on shear and top flange. Moreover, a small difference is observed for the concentrated load when load is on the bottom flange. The difference is not higher than 3%.
- Important results are obtained on the effect of the variation of the buckling moment in terms of the mode number.
    - Under distributed load, the increase of the buckling moment M_{cr} is very sensitive to load positions.
    - For the case of concentrated load, the effects of load position are present for odd number mode while for even number mode, the buckling moment is independent of load position.

One obtains for *k*=2 and k=4, the ratio is respectively 3.93 and 15.41 for the three load positions (Fig.9a-c). This important result is in agreement with the analytical solutions derived in (48).

- Under uniformly distributed load (Fig.8), the increase of the ratio $M_{cr}(k)/ M_{cr,ref}$ in the mode number 4 compared to the 1st mode reaches respectively 12.77, 13.30 and 13.86 for TF, SC and BF positions.
- In the concentrated load case (Fig.9), the improvement is higher. At mode 4, the ratio reaches the same value 15.41 for all the 3 load positions.
- One can assess obviously, that this important increase of the beam lateral buckling resistance when higher modes are considered can lead to more efficient improvement of the beam strength capacity against instability phenomenon.

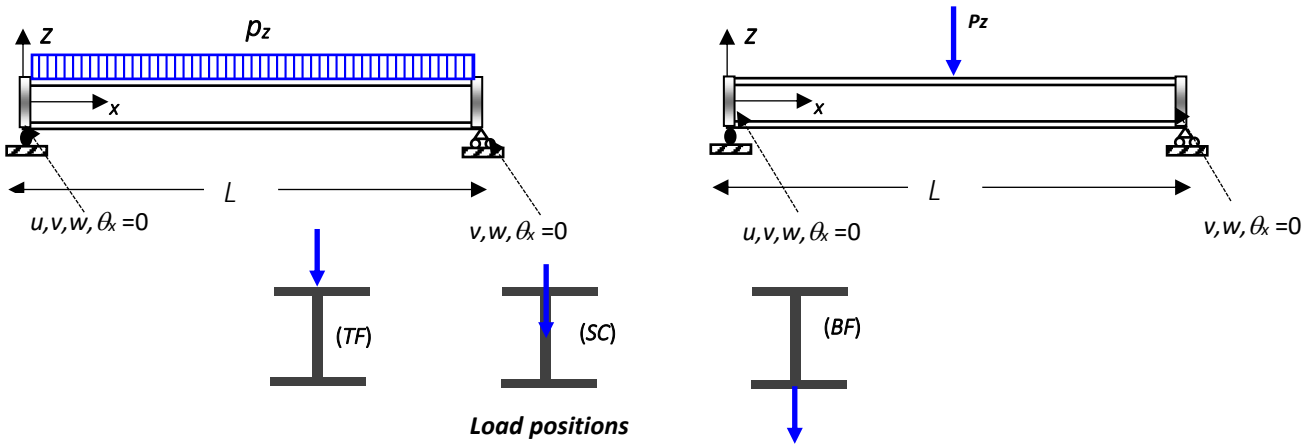

Fig.6: Simply supported beam under distributed and concentrated loads with load positions on top flange (**TF**), shear centre (**SC**) and bottom flange (**BF**).

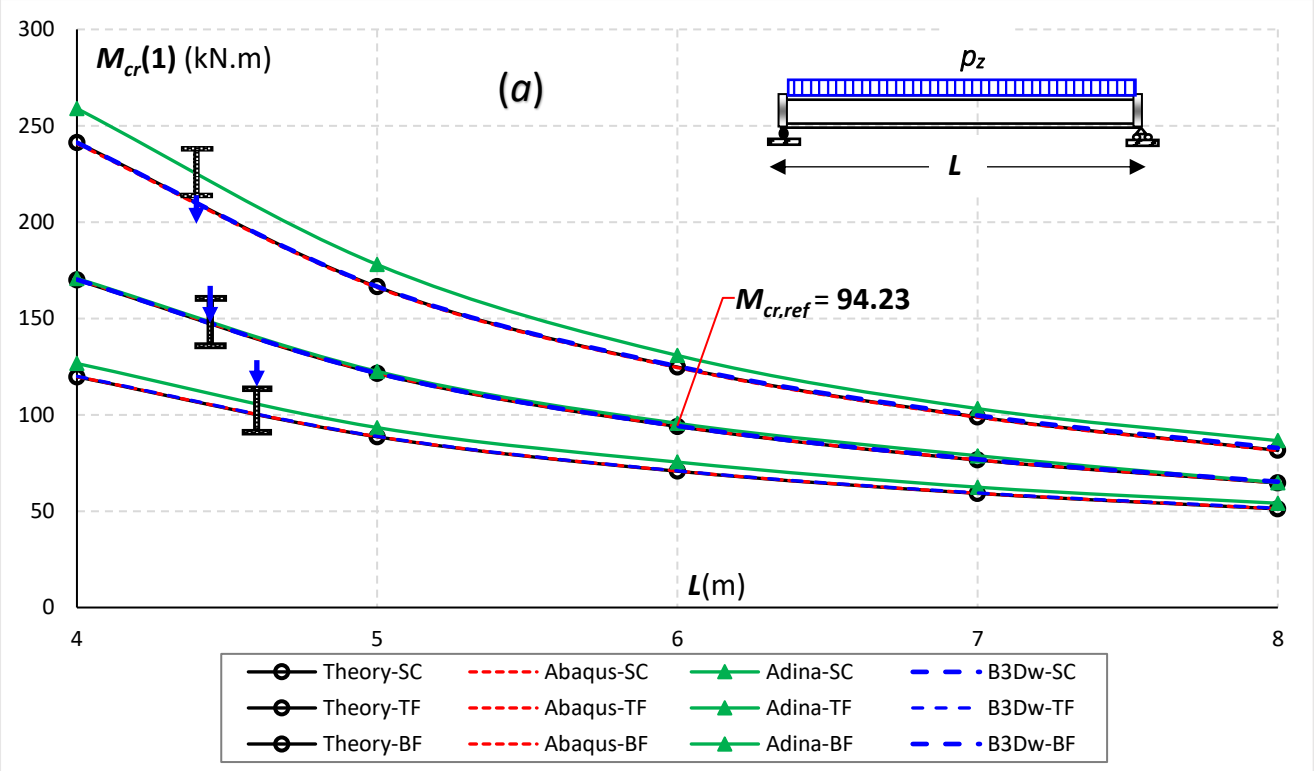

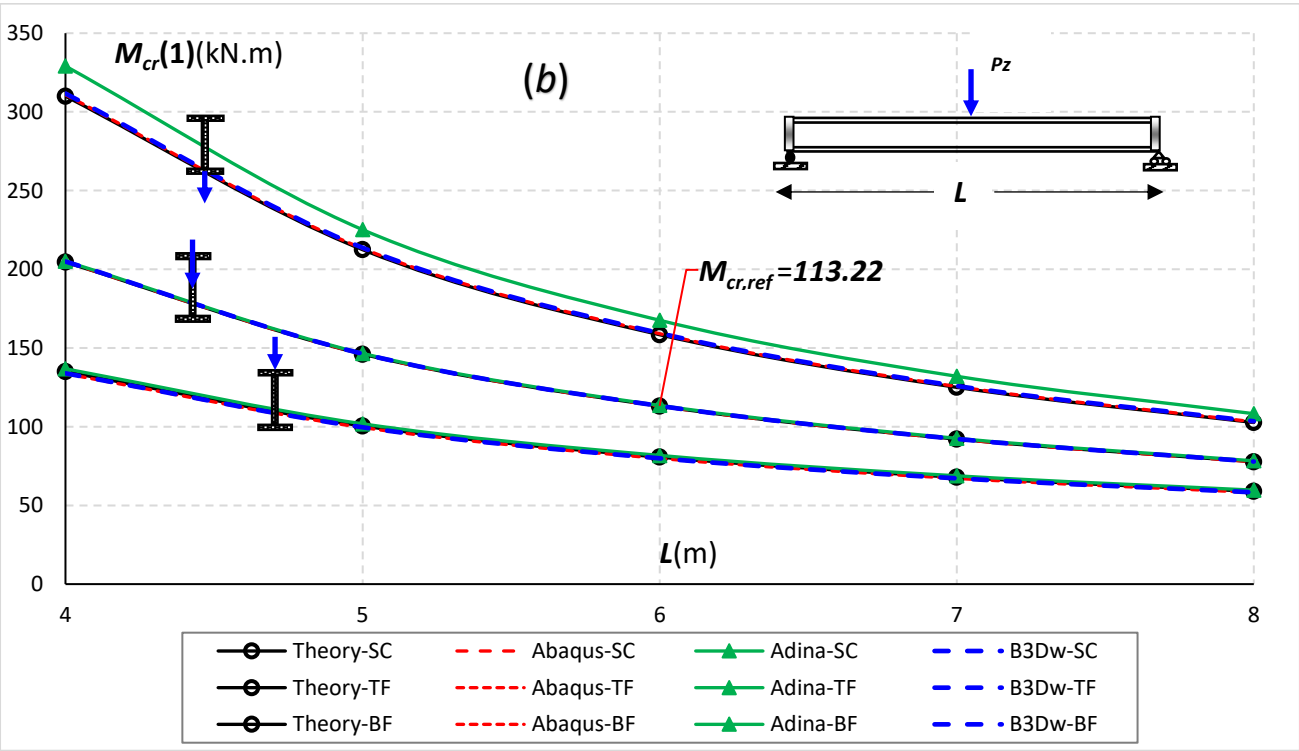

Fig.7: Variation of the lower buckling moments in terms of the slenderness ***L***. **(*a*)** uniformly distributed load, **(b)** concentrated load case.

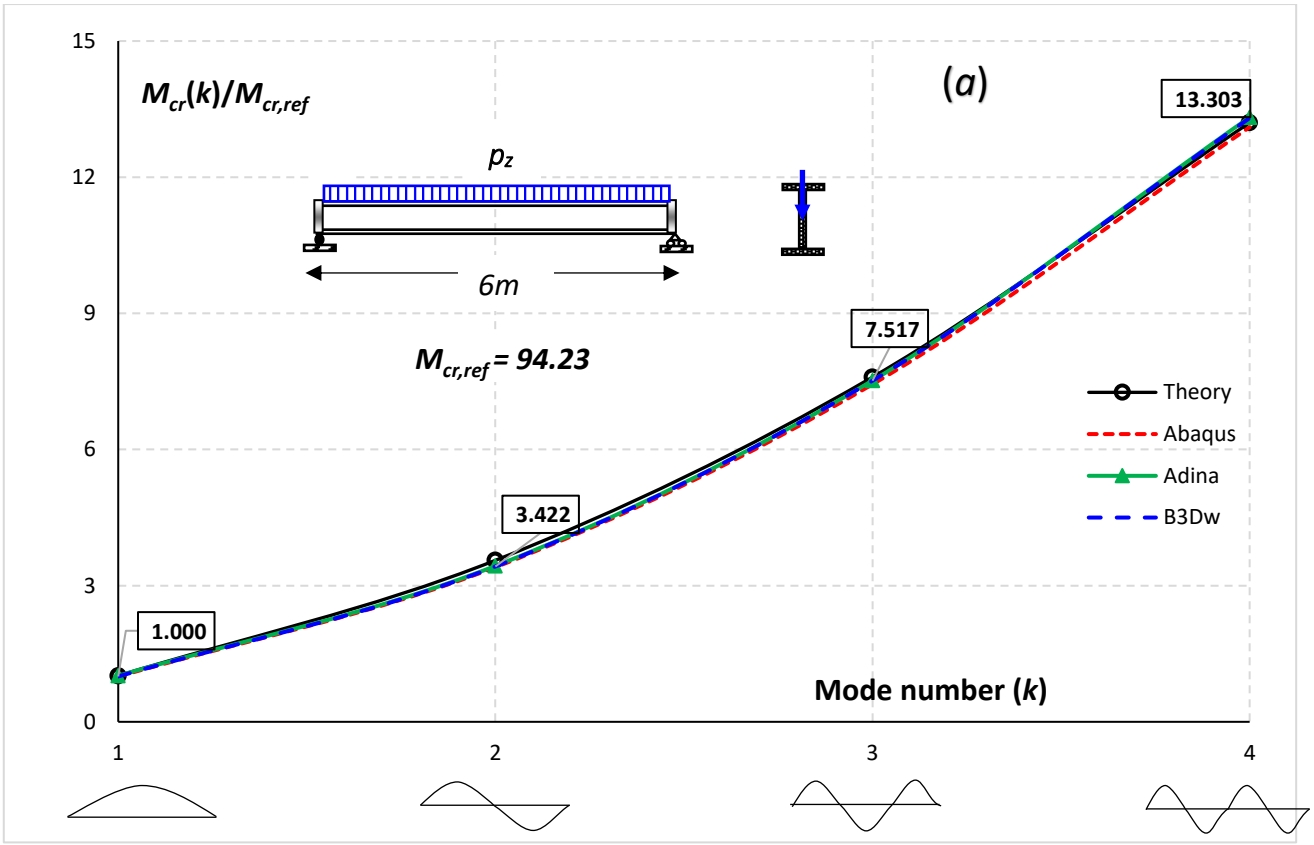
15
12
9
6
3
0
1
2
3
4
$M_{cr}(k)/M_{cr,ref}$
(a)
p_z
6m
$M_{cr,ref}$ = 94.23
13.303
7.517
3.422
1.000
Theory
Abaqus
Adina
B3Dw
Mode number (k)

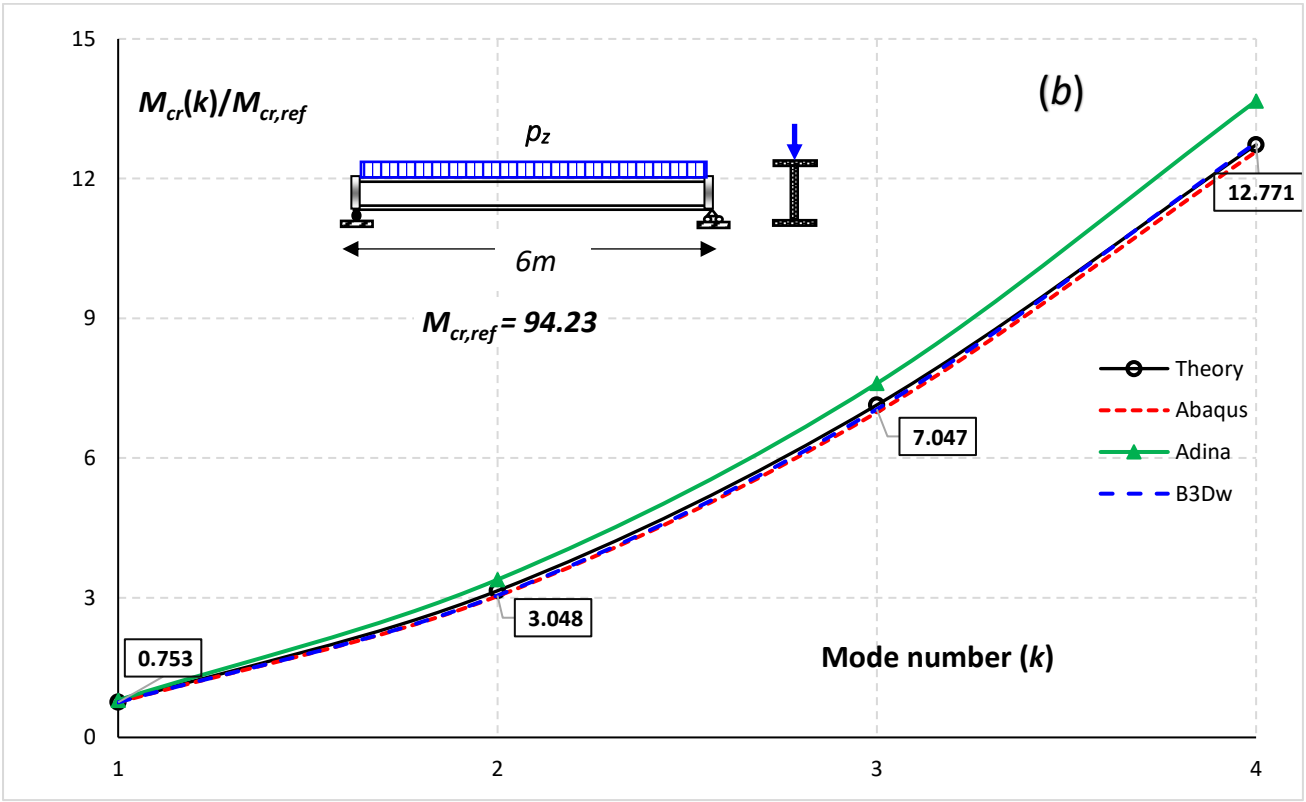
15
12
9
6
3
0
1
2
3
4
$M_{cr}(k)/M_{cr,ref}$
(b)
p_z
6m
$M_{cr,ref}$ = 94.23
12.771
7.047
3.048
0.753
Theory
Abaqus
Adina
B3Dw
Mode number (k)

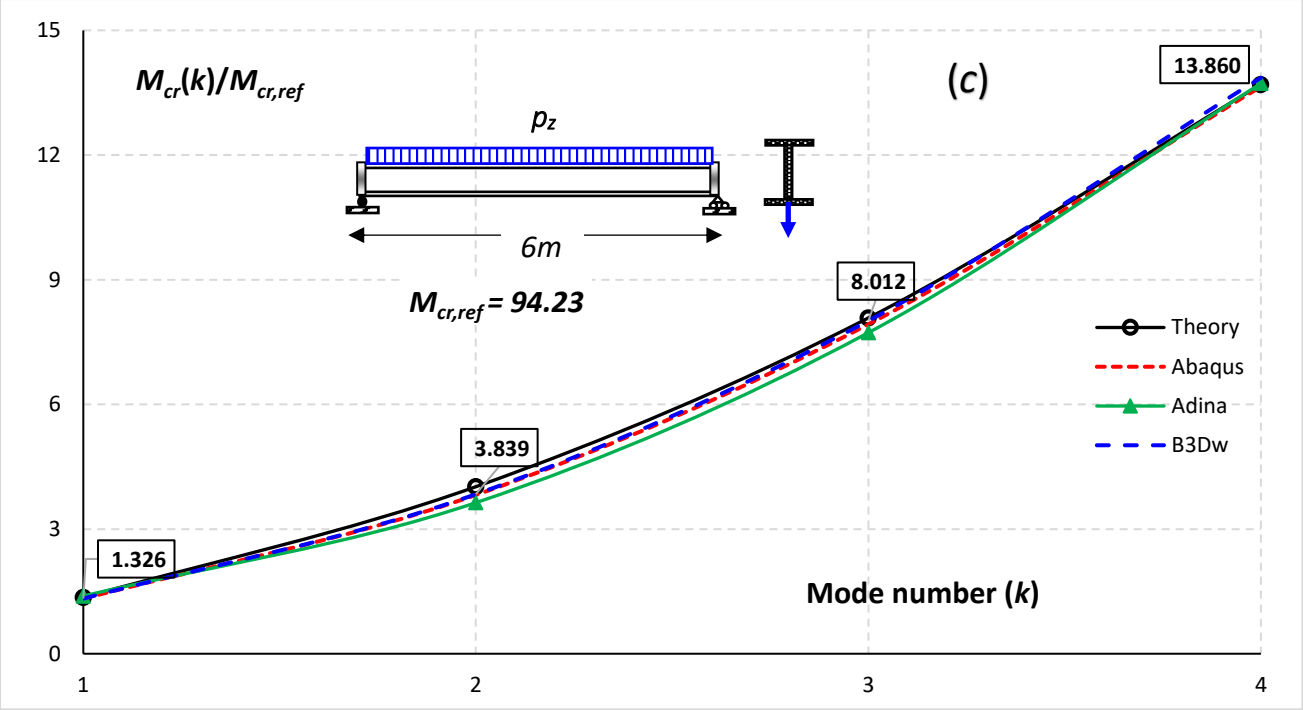

Fig.8: Doubly symmetric I beam under uniformly distributed load: theoretical and numerical buckling moments of the first four modes in terms of load height position and the mode number ***k***. ((*a*): SC, (*b*): TF and (*c*): BF)).

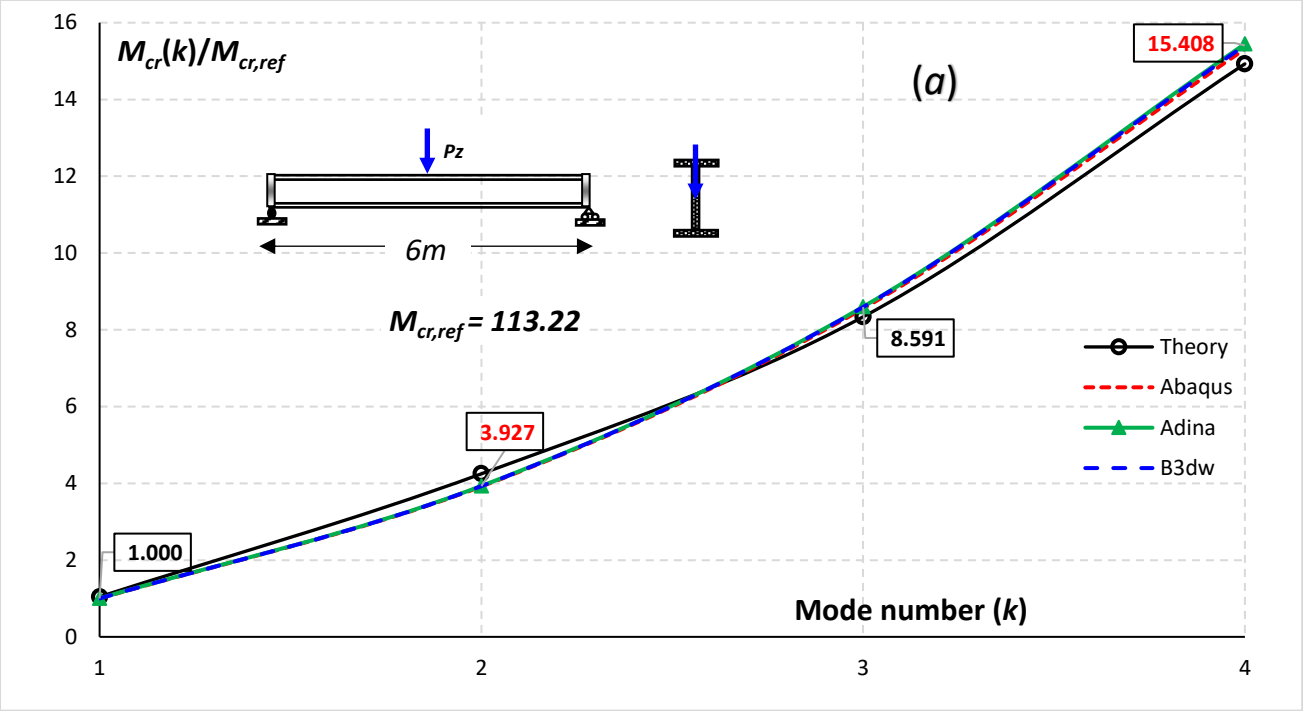
$M_{cr}(k)/M_{cr,ref}$
(a)
Pz
6m
$M_{cr,ref}$ = 113.22
15.408
8.591
3.927
1.000
Theory
Abaqus
Adina
B3dw
Mode number (k)
16
14
12
10
8
6
4
2
0
1
2
3
4

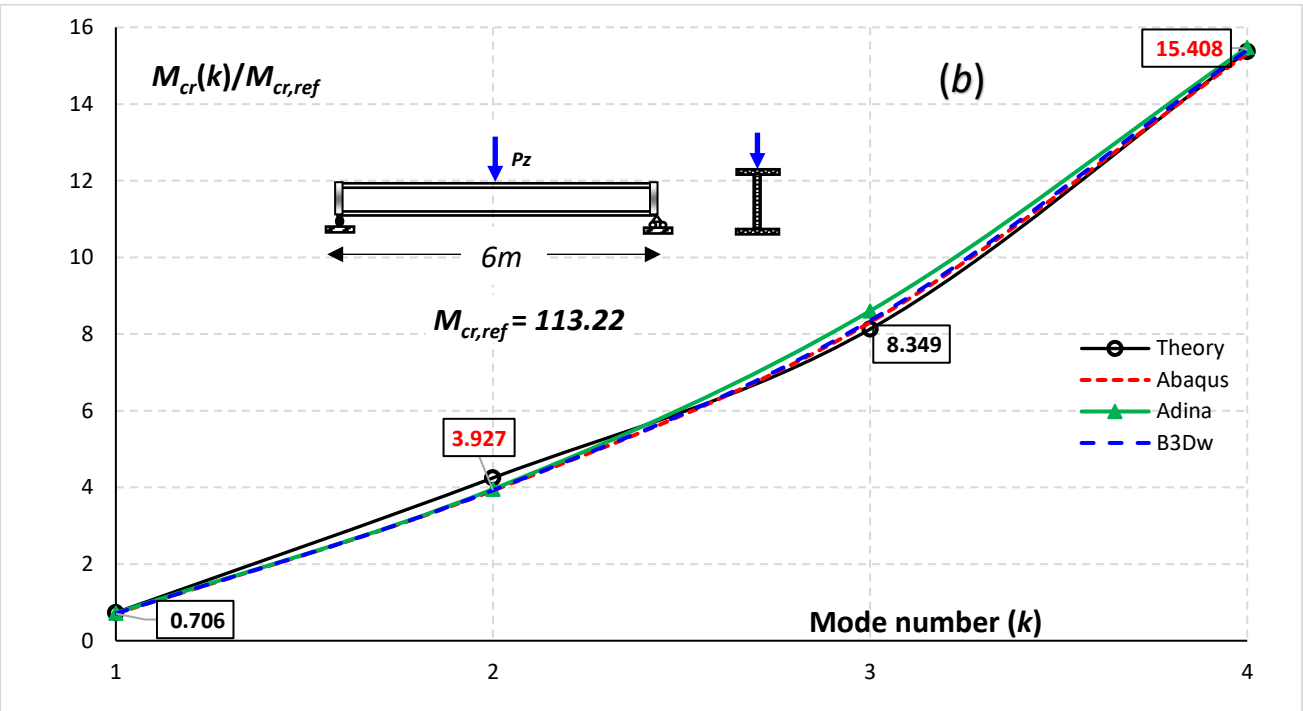
$M_{cr}(k)/M_{cr,ref}$
(b)
Pz
6m
$M_{cr,ref}$ = 113.22
15.408
8.349
3.927
0.706
Theory
Abaqus
Adina
B3Dw
Mode number (k)
16
14
12
10
8
6
4
2
0
1
2
3
4

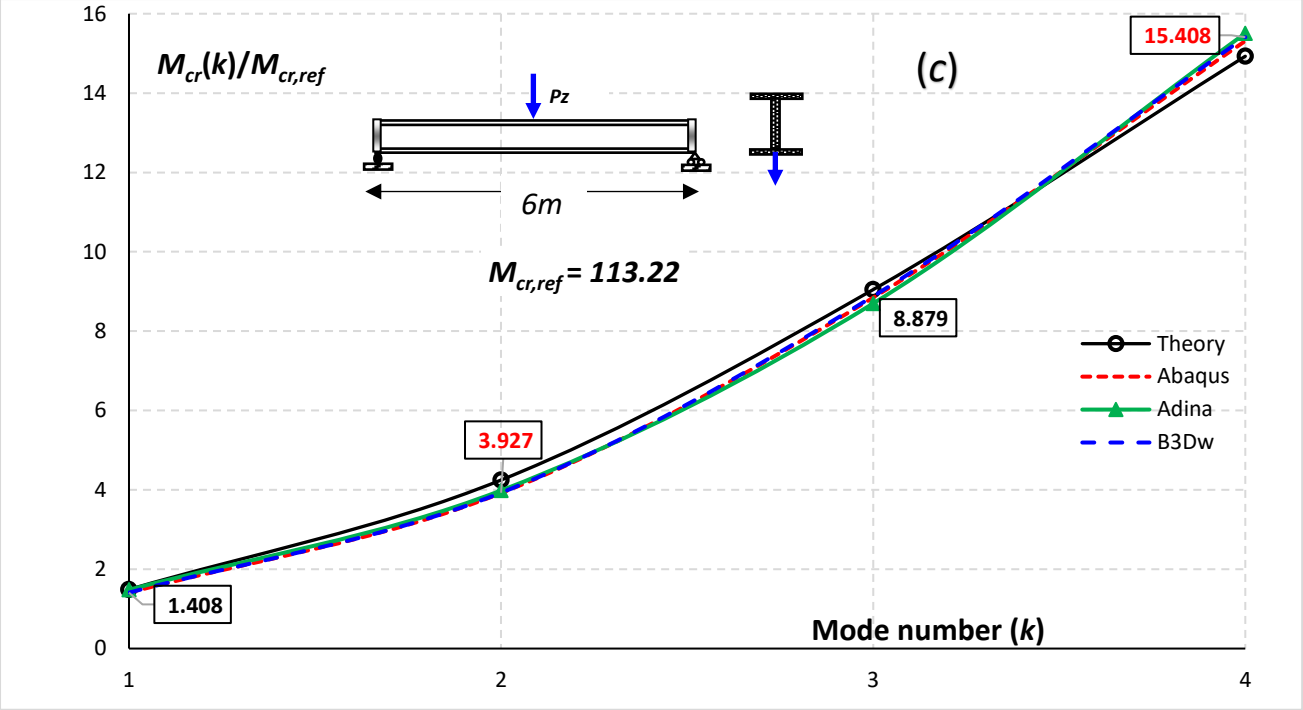

Fig.9: Doubly symmetric I beam under concentrated load, theoretical and numerical buckling moments of the first four modes in terms of load height position and mode number ***k***.
((a): SC, (b): TF and (c): BF)

In all the previous cases, there is an excellent agreement between the proposed methods (Analytical, FEM) and those obtained by Abaqus or Adina, confirming the accuracy and efficiency of the present methodology. Closed-form solutions are proposed for higher buckling loads. In more general cases, the finite element approach should be more efficient. In what follows, effects of higher buckling modes in design according to Eurocode 3 [27] are first discussed and applications of higher modes in buckling and lateral buckling strength capacity are presented.

5. Incidence of higher buckling loads on strength capacity

5.1.1 Buckling strength capacity

According to the Eurocode 3 (EC3) [27] adopted in Europe, for a column with a cross section ***A*** and a yield stress f_y, the strength capacity is computed in terms of the buckling loads according to the following relationship:

$$N_{b,rd} = \chi A f_y \quad (50)$$

The reduction factor χ is carried out in terms of the reduced slenderness $\bar{\lambda} = \sqrt{\frac{Af_y}{P_{cr}}}$ and the imperfection curves ϕ, given by:

$$\chi = \frac{1}{\phi + \sqrt{\phi^2 - \bar{\lambda}^2}} \qquad \text{Where } \phi = 0.5\left(1 + \alpha\left(\bar{\lambda} - 0.2\right) + \bar{\lambda}^2\right) \quad (51a,b)$$

α is an imperfection coefficient. It is function on the cross-section shape and the steel yield stress f_y. This coefficient is given for 5 reference curves denoted (***a₀, a, b, c, d***). To our knowledge, these curves are good only for imperfection and buckling in bending modes only (Euler's buckling). This means that the buckling analysis is under 2D assumption. The choice of the buckling curves is function on the cross-section shapes [EC3, Table 6.2]. As an example, in the case of an **I**-section with short flanges (classical I sections, for which the ratio ***h/b***>1.2), the curve ***a*** is used when $P_{cr} = P_z$ (i.e axis z-z). The curve *b* is chosen when $P_{cr} = P_y$ (i.e axis yy). For I section with large flanges *h/b* <1.2, the curves ***b*** and **c** are used respectively. In 3D buckling analysis, the buckling load should be either P_y, P_z or P_θ. In the last case, there is no recommendation for the choice of the imperfection curve that must be used when $P_{cr} = P_\theta$. Similar comment is true for the results of example 3 and 4 where all buckling modes are flexural-torsional. To our opinion, since the torsion stresses due to warping are more important than the bending stresses, it would be prudent and reasonable to adopt the curve ***d*** in the presence of pure torsion or flexural-torsional buckling modes. This decision will be considered hereafter. In order to evaluate the approach suggested in EC3 to treat buckling strength

of thin-walled elements and to illustrate the effect of higher buckling modes on strength capacity examples are presented herein. In the analysis, we admit that we are in presence of compact cross section (section class 4 not considered).

5.1.2 Examples

Example 1: Buckling of an unrestrained and braced simply supported beams

An unrestrained and restrained beam with a total length *L*=9m with a doubly symmetric cross-section, namely HP 400*122 *(**h**=34.80, **b**=39, t_f=1.40, t_w=1.40)* is considered. The steel grade S235 (f_y=235 MPa) is admitted. The strength of the beam is studied under unrestrained (Fig 10, case 1) and restrained conditions in presence of braces (Fig. 10, cases 2-4). In the last cases, the braces are located at the mid-height of the beam. To isolate the effect of bracing on the beam, null flexural and torsional rigidity are imposed at the assembly beam-bracing (i.e. full rigid bracings). The adopted boundary conditions at brace positions are illustrated in Fig.9. Linear buckling analyses are carried out using B3dw in order to examine the bracing effects on critical load values of the beams. These resulting buckling loads are used in design of the beam strength capacity according to EC3 strategy.

The buckling loads of the 4 cases are summarized in table 7. The analytical and the numerical buckling loads P_y, P_z and P_θ are reported for each load case. The buckling loads are used in the computation of the reduction buckling ratio χ according to (51). The bar strength capacity $N_{b,rd}$ are then obtained for each case. One can remark that for the unbraced beam (case 1), the bar buckles according to the first mode. The lower buckling modes are in bending about the weak axis followed by the torsion buckling load. Due to these modes buckling, the buckling ratio is near 0.53. The loss due to buckling is near **47%**. In presence of braces (cases 2-4), the bar buckles according to higher modes and the buckling loads increase accordingly. The bar strength is improved efficiency and the

loss is only **11%** in the last case. This value is acceptable and one can conclude that the buckling effect has been reduced a minimum. To reach this improvement, braces in all directions have been necessary.

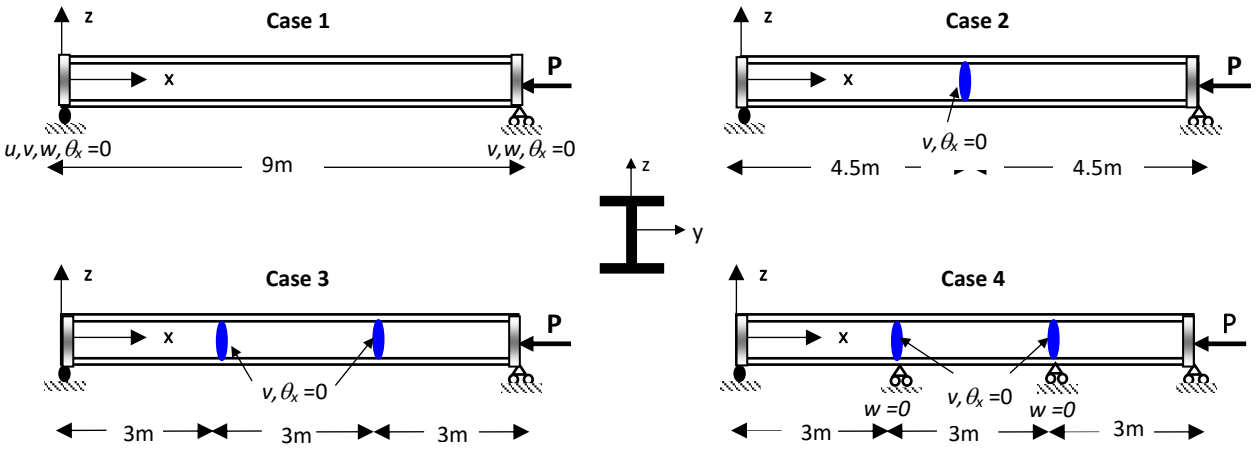

Fig. 10: Boundary conditions of unbraced and braced beams.

case	L_y	L_z	L_θ	Af_y	*Analytical*			*B3Dw*		
					P_y	P_z	P_θ	P_y	P_z	P_θ
1	9	9	9	3664.36	8896.81	3544.08	6133.80	8896.81	3544.08	6133.79
2	9	4 .5	4.5		8896.81	14176.33	15643.57	8896.81	14176.33	15643.57
3	9	3	3		8896.81	31896.75	31493.18	8896.81	31896.75	31493.18
4	3	3	3		80071	31896.75	31493.18	80071.32	31896.75	31493.18

	$\bar{\lambda}_y$	$\bar{\lambda}_z$	$\bar{\lambda}_\theta$	χ_y	χ_z	χ_θ	χ	$N_{b,rd}$ *present*	$\alpha_{cr}=P_{cr}/Af_y$	*Strength loss*
Tab (*cont*)	0.642	1.017	0.773	0.816	**0.530**	0.596	**0.530**	1942.11	0.97	47%
	0.642	0.508	0.484	0.816	0.838	**0.791**	**0.791**	2898.51	4.27	21%
	0.642	0.339	0.341	**0.816**	0.929	0.893	**0.816**	2990.12	2.43	18%
	0.214	0.339	0.341	0,99	0.929	**0.893**	**0.893**	3272.00	8.59	11%

Table 7: Buckling loads and strength capacity of unbraced and braced beam

Example 2: Buckling of an unrestrained and braced cantilever beams

In this example, effects of braces on buckling and strength of a cantilever beam are studied. At the clamped end of the beam, all displacements, rotations and warping are restrained. This means that the 7 DOFs of the origin are locked. The cross-section HEA 500 ($\boldsymbol{h}$=490, $\boldsymbol{b}$=300, $\boldsymbol{t_f}$=23, $\boldsymbol{t_w}$=12mm) is adopted in the study. The unstrained beam (Fig.11, case1) has a span $\boldsymbol{L}$=12 m. In addition, five bracing scenarios are investigated for the beam. Their positions with the conditions are illustrated in (Fig.11, case 2-6). For each case, the buckling loads are computed and the bar strength is found accordingly. For these cases, no accurate analytical solutions for 3D buckling loads are available. This is the reason why only numerical buckling loads are reported in table 8. They are obtained by the beam finite element presented in this model (B3Dw)**.** The buckling loads are used in the computation of the reduction buckling ratio χ according to (51). The bar strength capacity $\boldsymbol{N_{b,rd}}$ are then obtained for each case.

In the case of the unrestrained beam (case 1), the lower buckling load is about the weak axis z-z. This value is very low (P_z=373 kN). This leads to a very low reduction factor χ= χ_z=0.073. The loss due to buckling is very important (93%). When the braces are provided in cases 2 and 3, the bar strength has been improved and the loss due to buckling decreases to 54% and 48% respectively. Moreover, one remarks, that in case 3, the lower buckling is about the strong axis y (χ_{min} = χ_y=0.52). This means, that braces are needed in the 3 directions as adopted in the last cases (case 4-6). The strength of the column can be improved as in the case 6 where braces are positioned at 3, 6, 9 and 12m.In this last case, buckling effect on strength capacity is reduced at minimum (only 13% loss with regard to full strength).

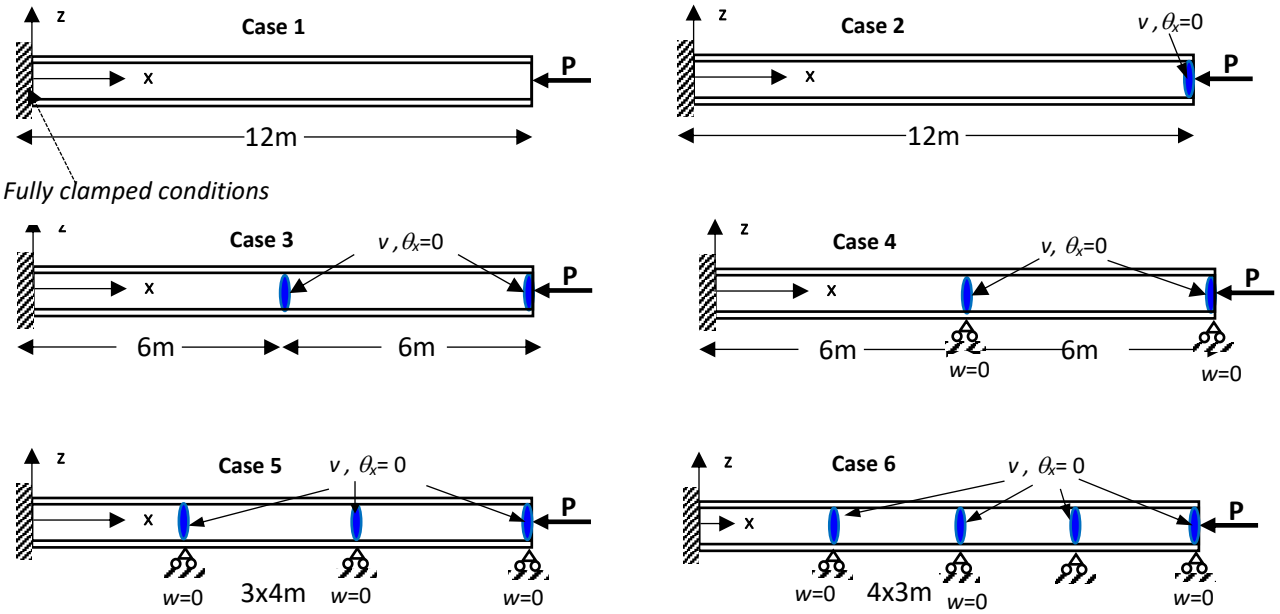

Fig. 11: Boundary conditions and position of unbraced and braced beams.

case	Af_y	*B3Dw*			$\bar{\lambda}_y$	$\bar{\lambda}_z$	$\bar{\lambda}_\theta$
		P_y	P_z	P_θ			
1	**4641**	3129.44	373.14	5480.75	1.218	3.527	0.920
2		3129.44	3053.43	8440.04	1.349	1.436	0.981
3		3129.44	7730.64	13604.13	1.218	0.775	0.584
4		25608.15	7730.64	13604.13	0.426	0.775	0.584
5		1277792	15237.47	21892.69	0.060	0.552	0.460
6		215635.60	25701.48	33446.18	0.15	0.42	0.37

Tab (cont)	χ_y	χ_z	χ_θ	χ	$N_{b,rd}$ *present*	$\alpha_{cr}=P_{cr}/Af_y$	*Strength loss*
1	0.519	**0.073**	0.509	**0.073**	339.80	0.08	93%
2	0.519	**0.461**	0.616	**0.461**	2137.90	0.66	54%
3	**0.519**	0.740	0.721	**0.519**	2408.26	0.67	48%
4	0.916	**0.678**	0.714	**0.678**	3146.58	1.66	28%
5	1	0.813	**0.801**	**0.801**	3719.39	4.71	20%
6	1	0.884	**0.866**	**0.866**	4019.32	7.20	13%

Table 8: Buckling loads and strength capacity of unbraced and braced cantilever beams.

5.2 Beam lateral buckling strength capacity

According to the Eurocode 3 (EC3) [27], The bending moment resistance of a beam in bending with lateral torsional buckling taken into account should be determined with:

$$\boldsymbol{M_{b,rd} = \chi_{LT}\, W f_y} \quad (52)$$

Value of the reduction factor χ_{LT} is functioned on non-dimensional slenderness $\bar{\boldsymbol{\lambda}}_{\boldsymbol{LT}} = \sqrt{\frac{\boldsymbol{W f_y}}{\boldsymbol{M_{cr}}}}$ and the imperfection curves $\boldsymbol{\phi}$ given in (51).

An evaluation of the effect of bracing on the lateral buckling capacity of a simply supported beam is of practical importance. For this aim, a thin-walled bisymmetric section (IPE500) beam with length $\boldsymbol{L}$ = 12 m is investigated in this example. Unbraced and braced beams are subjected to uniformly distributed load at positions SC, BF and TF. The geometry, with boundary conditions and position of braces are depicted in Fig. 12 for the studied cases (case1 to 4). The design buckling resistance moment $\boldsymbol{M_{b,rd}}$ are reported in Fig. 13 for each case and normalized to the full bending strength moment (M_{rd}=515.59 kNm). One remarks that in the unrestrained beam (case 1), the loss of bending strength due to lateral buckling is very important and depend on load position. It reaches respectively 75.70 and 65% for TF, SC and BF load positions. In presence of bracing, the beam strength increases non linearly in terms of the number of bracing and in presence of 3 braces, one observes that the loss is only 12%, for the all the load positions. The same study has been investigated for the same beam under concentrated load and the same boundary conditions as in Fig.12. The same tendency has been observed, but the improvement of the beam strength is best. In presence of 3 braces (case 4), the loss is only 9% (Fig.14).

The effect of braces in the improvement of beam strength against lateral buckling is then more evident and proven. Let us remind that effects of bracing in design are always based on empirical assumptions.

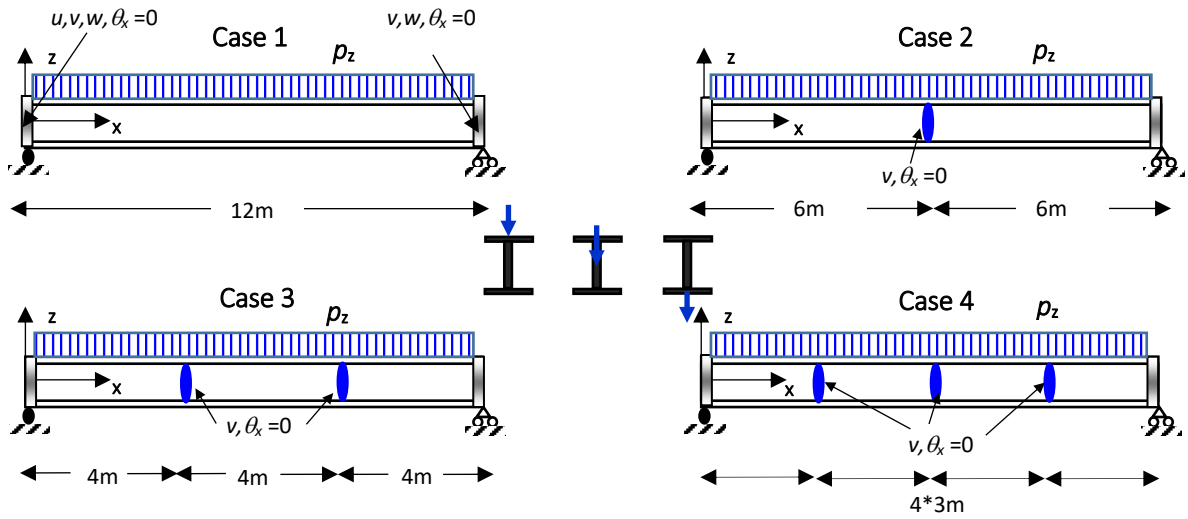

Fig. 12: Boundary conditions and position of unbraced and braced beams

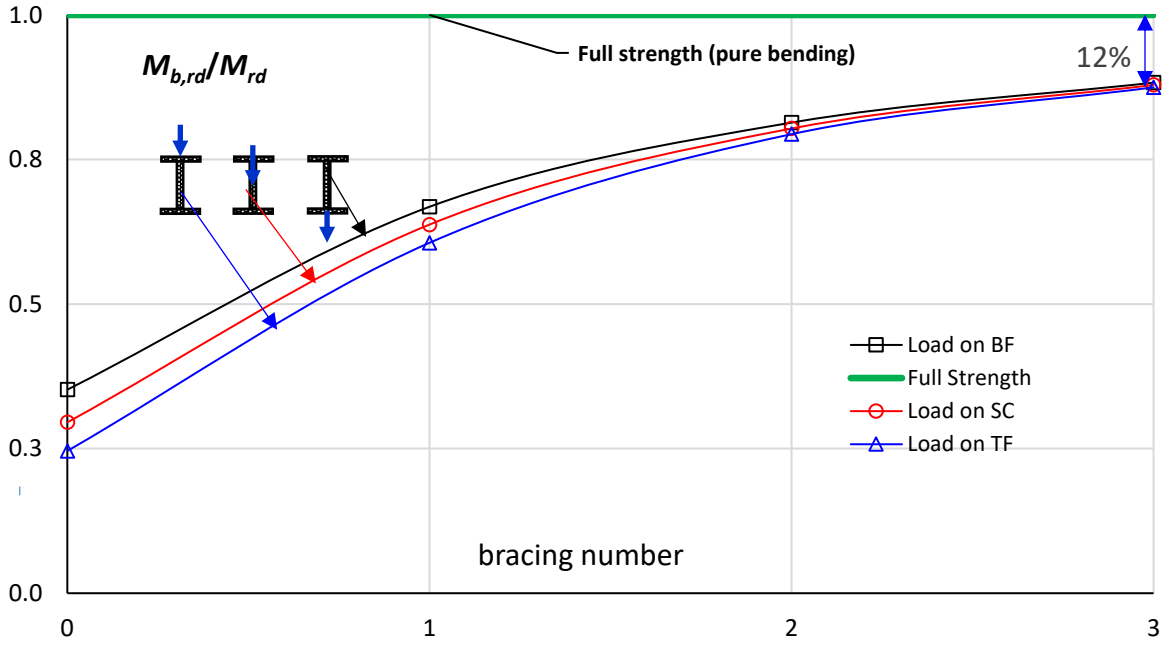

Fig.13: Beam under uniformly distributed load: Effect of bracing and load position on the lateral buckling strength capacity.

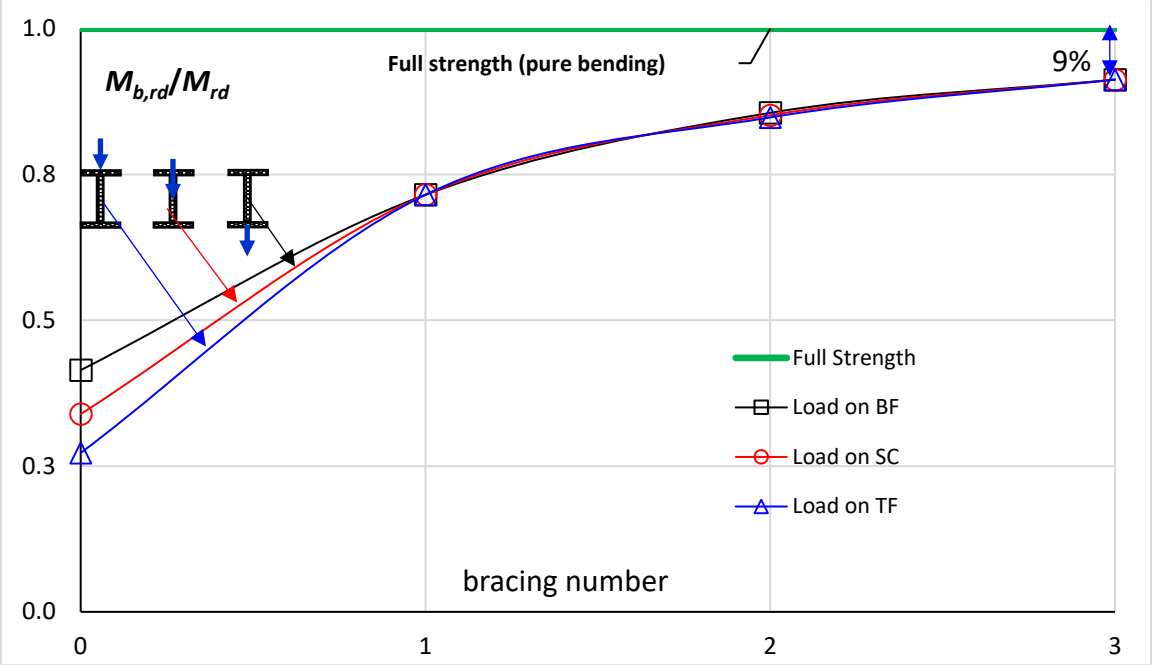

Fig.14: Beam under concentrated load: Effect of bracing and load position on the lateral buckling strength capacity.

Conclusion

Higher buckling and lateral buckling of beams with open cross sections have been investigated in the present work by analytical and the Finite Element Method approaches. Firstly, improved closed-form solutions for the buckling of bars according to higher buckling modes are derived for simply supported bars with singly symmetric cross-sections. For bars with arbitrary cross-section, a semi-analytical procedure is attempted. In lateral buckling, analytical solutions attempts have been carried out for higher lateral buckling moments of doubly symmetric I beam under uniformly and concentrated loads, the influence of load position on the stability of the beam has been included in the solution. The analytical and the FEM numerical results of the present model are compared to some available benchmark solutions of the literature and to finite element simulations of the commercial codes (Abaqus and Adina). The main conclusions of the present contribution can be drawn as follows:

- By including higher buckling modes, one assesses the behaviour of the unrestrained and the braced structures.
- For singly symmetric, bending or coupled flexural torsional modes should be present.
- For arbitrary cross sections, fully coupled flexural-torsional modes control the buckling.
- The present model is in good agreement with benchmark solutions. The analytical solutions are original and concord well with the numerical simulations.
- The large number of numeric examples shown that B3Dw element is successful in higher buckling analyses in presence of arbitrary cross sections and any boundary conditions, where analytical solutions fail and are limited to simple cases.
- In buckling strength, the Eurocode 3 solutions are limited to classical bending buckling modes. Some improvements are proposed in the present study in presence of torsion modes.
- In lateral buckling, original results are obtained when higher modes are considered. Under distributed load case, the increase of the buckling moment M_{cr} is very sensitive to load positions and mode number. However, for the case of concentrated load, the effects of load position are present for odd number mode while for even number mode the buckling moment M_{cr} is independent to load position.
- Finally, it can be concluded that consideration of higher buckling modes are very important in design. They can help the understanding of the behaviour of the braced beams in presence of stability phenomena. Effect of braces can be assessed accurately. Their number, their directions and positions can be optimized in order to control the stability problem and to cover the full strength of bar structures.

References

[1] Timoshenko SP, Gere JM, Theory of elastic stability, 2nd Ed, New York, McGraw Hill Inc, 1961,

[2] Jones RM, Buckling of bars, plates and shells, Bull Ridge Publishing, 2006

[3] Vlasov VZ, Thin-walled elastic beams, Moscow (French translation: Pieces longues en voiles minces), Eyrolles, Paris, 1962

[4] Bleich F, Buckling strength of metal structures, New York: McGraw-Hill, 1952

[5] Galambos TV, Guide to stability design criteria for metal structures, 1st Ed, New York: John Wiley & Sons Inc, 1998

[6] Murray NW Introduction to the theory of thin-walled structures, Clarendon Press, 1984

[7] Chen WF, Atsuta T , Theory of beam columns, vol 2, J Ross Publishing 2008.

[8] Librescu L, Song O Thin-Walled Composite Beams: Theory and Application, Springer, 2006,

[9] Papp F, Rubert A, Szalai J, DIN EN 1993-1-1-konforme integrierte Stabilitätsanalysen für 2D/3D-Stahlkonstruktionen (Teil 2), Stahlbau, 83, 2014.

[10] Yu Z, Bin H, Li-Ke Y and Jin L, Buckling analysis of thin-walled members via semi-analytical finite strip transfer matrix method, Advances in Mechanical Engineering 2016, 8(5), 1–11.

[11] Badari B, Papp F, On Design method of Lateral-torsional buckling of beams: State of the art and a new proposal for a general type Design Method, Periodica polytechnica civil engineering 2015, 59(2), 179-192.

[12] Flint AR. The influence of restraint on the stability of beams, The Structural Engineer, 1951, 29(9), 235-246.

[13] Winter G, Lateral Bracing of columns and beams, Transactions of the American Society of Civil Engineers (1960), 125(1), 807-826,

[14] Taylor A C, Ojalvo M, Torsional Restraint of Lateral Buckling, Journal of the structural division 1966, 92(2), 115-130,

[15] Kitipornchai, S, and N, J, Richter . Elastic lateral buckling of I-beams with discrete intermediate restraints, Civil engineering transactions, Institution of Engineers,1978, Australia CE20(2), 105-111,

[16] Trahair, N, S. Flexural-Torsional Buckling of Structures, CRC Press, USA, 1993.

[17] Yura, J. Fundamentals of beam bracing, Engineering Journal, AISC (First Quarter), 2001, 11-26.

[18] Nguyen CT, Moon J, Le VN, Lee HE. Lateral–torsional buckling of I-girders with discrete torsional bracings," Journal of Constructional Steel Research, 2010, 66(2), 170-177.

[19] McCann F, Gardner Land Wadee MA. Design of steel beams with discrete lateral restraints, Journal of Constructional Steel Research, 2013, 80(0): 82-90.

[20] Agüero A, Pallarés F,J, Pallarés L. Equivalent geometric imperfection definition in steel structures sensitive to lateral torsional buckling due to bending moment, Engineering Structures, 96, 2015, 160–177.

[21] Zhang WF, Liu YC, Hou G, Chen KS, Ji J, Deng Y, and Deng SL. Lateral-torsional buckling analysis of cantilever beam with tip lateral elastic brace under uniform and concentrated load, International Journal of Steel Structures 2016, 16(4): 1161-1173.

[22] Pezeshky P, Sahraei A and Mohareb M Effect of bracing height on lateral torsional buckling resistance of steel beams, 6th International Conference on Engineering Mechanics and Materials, Vancouver, 2017.

[23] Cescotto S, Massonet C. Mécanique des matériaux, De Boeck, 3e Ed, 1994.

[24] Akesson B. Plate buckling in bridges and other structures, Taylor&Francis Group 2007.

[25] Degenhardt R, Rolfes R, Zimmermann R, Rohwer K: COCOMAT: Improved material exploitation at safe design of composite airframe structures by accurate simulation of collapse, Composite Structures, 2006, 73, 175-17

[26] Zimmermann R, Klein H, Kling A. Buckling and Post-buckling analysis of stringer stiffened fibre composite curved panels, Composite Structures, 2006,73, 150-161.

[27] Eurocode 3: European Committee for Standardization, EN 1993-1-1, Eurocode 3: Design of steel structures, Part 1-1: General rules and rules for buildings, Brussels, May 2005.

[28] Eurocode 4: Design of composite steel and concrete structures – Part 1-1: General rules and rules for buildings,

[29] Eurocode 5: Design of timber structures - Part 1-1: General - Common rules and rules for buildings

[30] Abaqus/CAE Analysis, Simulia, 2011, version 6.11, Dassault System.

[31] Mohri F, Azrar L and Potier-Ferry M. Flexural-torsional post-buckling analysis of thin-walled elements with open sections, Thin-Walled Structures, 2001, 39, 907-938.

[32] Mohri F, Damil N, Potier-Ferry M. Large torsion finite element model for thin-walled beams, Computers and Structures 2008, 86, 671–683.

[33] Mohri F, Brouki A, Roth JC. Theoretical and numerical stability analyses of unrestrained, mono-symmetric thin-walled beams, Journal of Constructional Steel Research 2003, 59, 63–90.

[34] Mohri F, Damil N, Potier-Ferry M. Review and comparison of finite element flexural–torsional models for non-linear behaviour of thin-walled beams, Advances in Engineering Software 2015, 80, 174-187.

[35] Matlab^{R} 2014a: The Mathworks Inc, 2014.

[36] Adina (2011): Theory and Modelling Guide - Volume I: Adina Solids & Structures, Adina R & D, Inc, 71 Elton Avenue Watertown, MA 02472 USA, December 2012.

[37] Schafer B W.Thin-walled column design considering local, distortional and Euler buckling. Journal of Structural Engineering, ASCE, 2002, 128, 3, 289-299.

[38] Qiao P, Zou G, Davalos JF. Flexural–torsional buckling of fiber-reinforced plastic composite cantilever I-beams. Composite Structures 60 (2003) 205–217.

[39] Mascolo I, Modano M, Fiorillo A, Fulgione M, Pasquino V, Fraternali F. Experimental and Numerical Study on the Lateral-Torsional Buckling of Steel C-Beams with Variable Cross-Section Metals - Open Access Metallurgy Journal, November 2018, 8(11):941.

[40] Schafer B W, Review. The Direct Strength Method of cold-formed steel member design, Journal of Constructional Steel Research, 2008 64 (7), 766-778.

[41] Becque J, Rasmussen KJR, A. Numerical investigation of local-overall interaction buckling of stainless steel lipped channel columns, Journal of Constructional Steel Research, 65 (8–9) (2009) 1685–1693.

[42] Dinis PB, Camotim D. Local/distortional mode interaction in cold-formed steel lipped channel beams, Thin-Walled Structures, 48 (2010) 771–785.

[43] Hauksson HI Vilhjálmsson JB. Lateral-Torsional Buckling of Steel Beams with Open Cross Section, Thesis, Chalmers University Sweden, 2014.

APPENDIX

Figure A.1-3 depict the first four mode shapes of the 4m columns with channel section, Tee cross section and arbitrary cross section. In the column with channel section (Fig.A1), pure bending modes are present in mode 1 and 4. The second and the third are flexural torsional modes (*w* and θ_x coupled). In the column Tee section (Fig.A2), all modes are flexural torsional modes (*v* and θ_x coupled). No pure bending mode is present. The mode shapes of the column with arbitrary cross section (Fig.A3) are all flexural-torsional. All displacements are present (*v*, *w* and θ_x coupled).

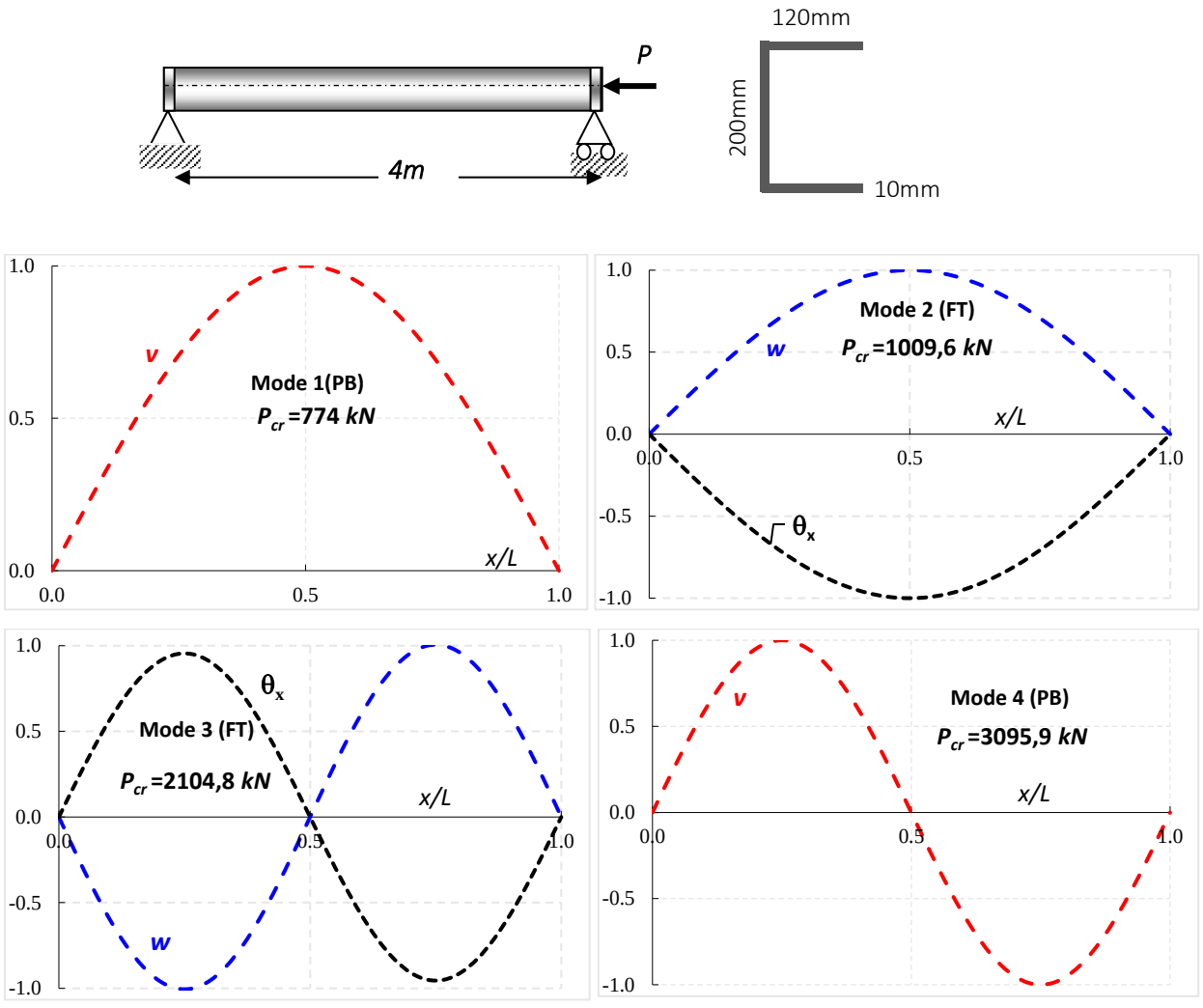

Fig. A1: Bar with Channel cross-section, the first four buckling mode shapes (B3Dw element).

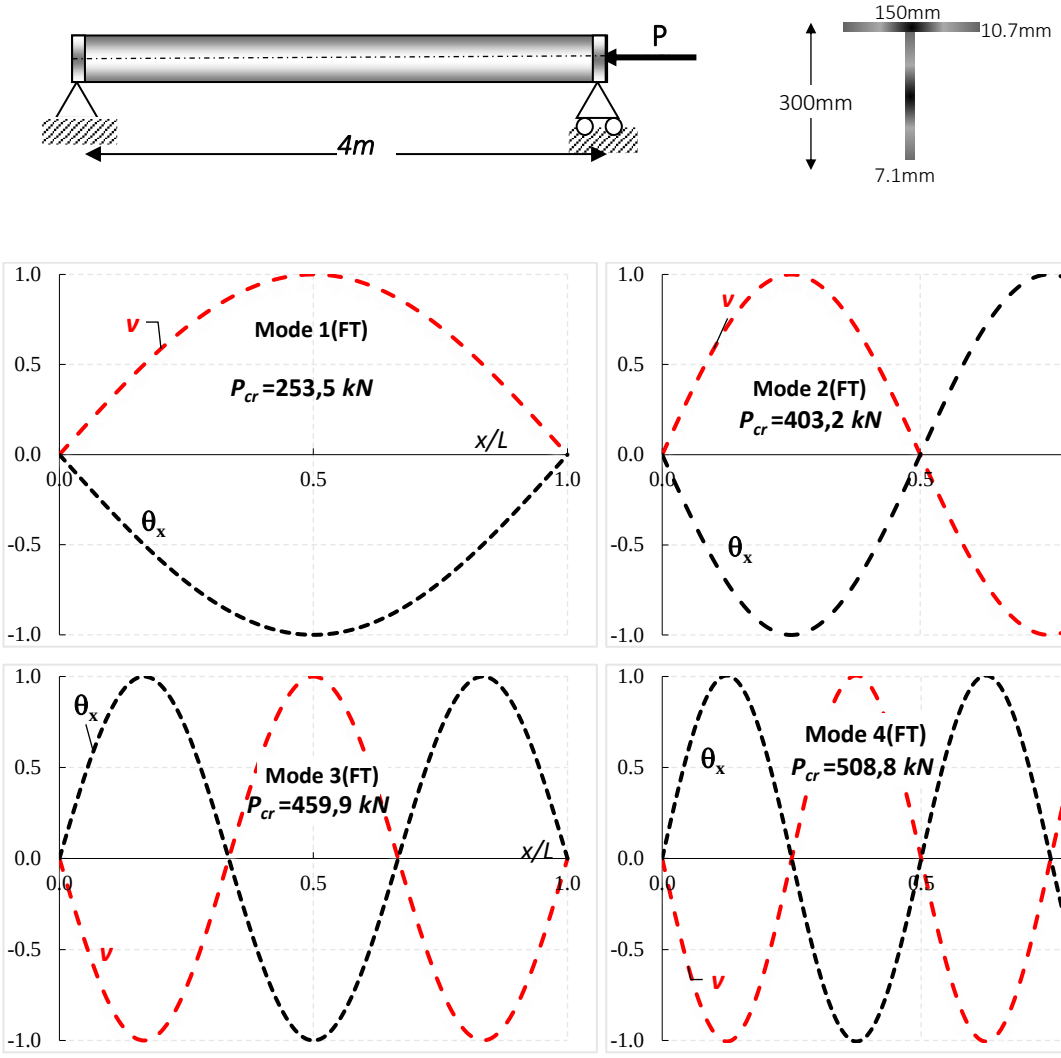

Fig. A2: Bar with Tee cross-section, the first four buckling mode shapes (B3Dw element).

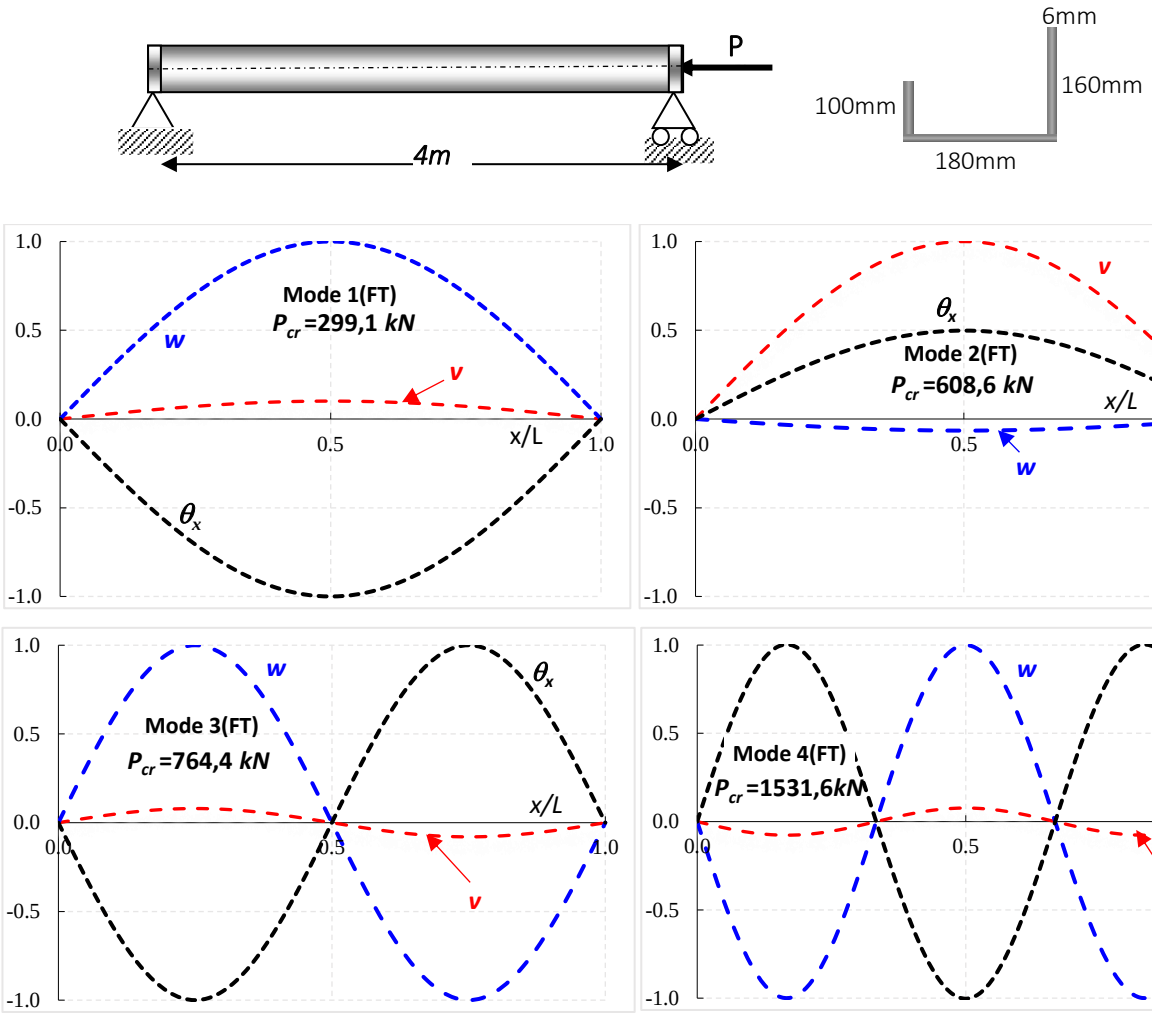

Fig. A3: Bar with arbitrary cross-section, the first four buckling mode shapes (B3Dw element).